공학박사학위논문

Surface Modified Silicon Electrode for Li-ion Batteries

표면 개질된 리튬 이차전지용 실리콘 전극

2013 년 2 월

서울대학교 대학원

재 료 공 학 부

화 윤

Abstract

Surface Modified Silicon Electrode for Li-ion Batteries

Yoon Hwa

Department of Materials Science and Engineering

The Graduate School

Seoul National University

Nowadays, energy storage and retrieve system are important issues to solve energy problems. There are many energy storage systems such as Pb-acid, Ni-Cd, Li-S and Li-ion batteries. Among them, Li-ion battery is one of the most viable candidates for energy storage due to its high energy and high power density. At present, conventional Li-ion batteries employ a carbonaceous material for anode material. But, it is not suitable for the new large unit applications due to due to its low specific capacity and poor rate capability. For this reason, it is necessary to develop advance anode materials for Li-ion batteries.

To overcome the limitations of carbonaceous materials, many researchers are paying attention to find other candidates replacing the graphite. Most of all, Si based systems are definitely attractive candidate for replacing the carbonaceous electrode due to the large theoretical specific capacity at room temperature ($Li_{15}Si_4$: 3600 mAh g^{-1}) and low operating voltage (near 0.1 V vs. Li/Li^+). However, in general, most Si based electrodes suffer from a large volume change during cycling and have a poor rate capability. The stress induced by a large volume change during the cycling cause pulverization of Si which leads to loss of electrical contact with current collector and formation of solid electrolyte interphase (SEI) layer on the electrode surface repetitively.

In this work, conducting carbon and SnO_2 were coated on Si nanoparticles for enhance the electrochemical properties of Si electrode, respectively. Conformal conducting carbon is one of the most famous coating material for enhance the electrochemical properties of electrode, and SnO_2 is a one of the promising candidate as anode materials for Li-ion batteries due to its excellent electrochemical performance. By combining those materials with Si, respectively, Si based electrode can be utilized fully in the anodes of Li-ion batteries. As a result of electrochemical test,

each electrodes showed excellent electrochemical behaviors. And also reaction mechanism of each electrodes was confirmed by various analyses. These core-shell nanostructured electrodes could be a strong candidate as an anode materials for Li-ion batteries.

Keywords : Li-ion batteries, Anode materials, Silicon, Core-shell structure, Electrochemistry, SnO_2, Carbon.

Student ID : 2007-20752

Contents

Abstract ---- **i**
Contents ---- **iv**
List of Figures ---- **vi**
List of Tables ---- **x**
Chapter 1. Introduction ---- **1**
Chapter 2. Theoretical Background ---- **6**
2.1 Fundamental of Rechargeable Li-ion Batteries ---- **6**
2.1.1 History ---- **6**
2.1.2 Principle ---- **8**
2.1.3 Terminology ---- **8**
2.2 Components of Rechargeable Li-ion Batteries ---- **13**
2.2.1 Anode ---- **13**
2.2.2 Cathode ---- **16**
2.2.3 Electrolyte ---- **17**
2.3 Silicon ---- **18**
2.4 Core-shell Nanostructured Materials ---- **24**
Chapter 3. Experimental ---- **27**
3.1 Electrode Preparation ---- **27**
3.1.1 Active Materials Preparation ---- **27**
3.1.2 Electrode and Cell Assembly ---- **28**
3.2 Electrochemical Test ---- **30**
3.2.1 Galvanostatic Test ---- **30**
3.2.2 Differential Capacity Plot (DCP) ---- **31**
3.3 Material Characterization ---- **31**
3.3.1 X-ray Diffraction (XRD) ---- **31**
3.3.2 Scanning Electron Microscope (SEM) ---- **33**
3.3.3 Transmission Electron Microscope (TEM) ---- **34**

Chapter 4. Results and Discussion ---- **39**
4.1 nano-Si/C Core-shell Material ---- **39**
4.1.1 Material Characterization ---- **39**
4.1.2 Electrochemical Characterization ---- **40**
4.2 nano-Si/SnO2 Core-shell Material ---- **58**
4.2.1 Material Characterization ---- **58**
4.2.2 Electrochemical Characterization ---- **58**
Chapter 5. Conclusions ---- **78**
References ---- **82**
Abstract (Korean) ---- **95**
감사의 글 **(Korean)** ---- **97**

List of Figures

Figure 1. The principle of operation of the first commercialized Li-ion batteries.

Figure 2. Chemical structures of solvent, (a) EC, (b) PC and co-solvent (c) DEC, (d) DMC, and (e) EMC as electrolyte for LiBs.

Figure 3. Schematic illustration of principles of XRD.

Figure 4. Schematic illustration of principles of SEM.

Figure 5. Schematic illustration of principles of TEM.

Figure 6. X-ray diffraction patterns of various electrodes samples.

Figure 7. FESEM image of nano-Si/C core-shell nanostructured material.

Figure 8. Schematic illustration and bright field TEM image of nano-Si/C core-shell nanostructured material.

Figure 9. (a) Bright field TEM image and (b) HRTEM image of nano-Si/PVA, respectively.

Figure 10. (a) Bright field TEM image and (b) HRTEM image of nano-Si/C core-shell nanostructured material, respectively.

Figure 11. Voltage profiles of nano-Si/PVA and nano-Si/C core-shell

nanostructured electrodes.

Figure 12. *Ex situ* XRD analysis of the first cycle (pristine, lithiated to 0.0 V, delithiated to 1.5 V).

Figure 13. *Ex situ* HRTEM images with SAED of the 1st cycle (a) discharged (lithiated to 0.0 V) and (b) charged (delithiated to 1.5 V) states, respectively.

Figure 14. Comparison of cyclability of nano-Si, nano-Si/PVA and nano-Si/C core-shell nanostructured electrodes at the constant current of 100 mA g^{-1}.

Figure 15. *Ex situ* TEM image with SAED of nano-Si/C core-shell nanastructured electrode of the 20th cycle at fully charge state to 1.5 V.

Figure 16. Rate capability test of nano-Si/C core-shell nanostructrued electrode at the various current rates (100 mA g^{-1}, 200 mA g^{-1}, 500 mA g^{-1}, 1000 mA g^{-1}, 1500 mA g^{-1}).

Figure 17. XRD patterns of nano-Si and nano-Si/SnO_2 core-shell nanostructured material.

Figure 18. (a) TEM image and (b) EDS concentration profiles for Si and Sn of nano-Si/SnO_2 core-shell nanostructured material. (c) TEM image of

SnO_2 hollow sphere.

Figure 19. Voltage profiles of (a) nano-Si/SnO_2 core-shell nanostructured, (b) nano-Si and (c) SnO_2 hollow sphere electrodes for the first cycle.

Figure 20. Ex situ analyses of nano-Si/SnO_2 core-shell nanostructured electrode. (a) DCP of the nano-Si/SnO_2 core-shell nanostructured electrode for the first cycle. (b) XRD results during the first cycle. Lithiation process: (I) 0.82 V, (II) 0.43 V, (III) 0.12 V, (IV) 0.0 V, Delithiation process: (V) 0.82 V, (VI) 2.50 V.

Figure 21. HRTEM images with SAED patterns of the nano-Si/SnO_2 core-shell nanostructured electrode. Lithiation process: (a) 0.82 V, (b) 0.43 V, (c) 0.12 V, (d) 0.0 V.

Figure 22. HRTEM images with SAED patterns of the nano-Si/SnO_2 core-shell nanostructured electrode. Lithiation process: (e) 0.0 V, dried and heat-treated at 500 ℃ for 12 h under Ar atmosphere.

Figure 23. HRTEM images with SAED patterns of the nano-Si/SnO_2 core-shell nanostructured electrode. Delithiation process: (a) 0.82 V, (b) 2.50 V.

Figure 24. Schematic illustration of reaction mechanism of nano-Si/SnO_2

core-shell nanostructured electrode.

Figure 25. Comparison of cyclabilities for the nano-Si and nano-Si/SnO_2 core-shell nanostructured electrodes.

Figure 26. (a) TEM image and (b) EDS mapping images of nano-Si/SnO_2 core-shell nanostructured electrodes of the 50th cycle at 2.5 V

Figure 27. Rate capability test of nano-Si/SnO_2 core-shell nanostructured electrodes at the various current rates (0.1 A g^{-1}, 0.2 A g^{-1}, 0.5A g^{-1}, 1 A g^{-1}, 1.5 A g^{-1}).

List of Tables

Table 1. The history of batteries.

Table 2. Maximum theoretical capacity of various Li-M alloys.

Table 3. Characteristics of representative cathode materials for LiBs.

Table 4. The characteristics of various solvent and salts as electrolyte for LiBs.

Chapter 1. Introduction

In contemporary society, the development of advanced energy storage system is certainly one of the most important issues owing to the increasing demand of portable electronic devices and electrical vehicles (EVs). To meet the demands, many energy storage systems such as Pb-acid, Ni-Cd, Ni-metal hydride, Li-S, Li-air and Li-ion batteries have been researched intensively.[1-12] Among them, Li-ion battery is one of the most viable candidates for energy storage due to its high energy and high power density.[1,13] Commercialized Li-ion system, consisting of graphite (LiC_6 : 372 mAh g^{-1})[3] as anode material and $LiCoO_2$ (ca. 140 mAh g^{-1})[3] as cathode material.[14-16] However, existing conventional Li-ion systems still have not met the needed power, and the gap between the energy consumption of portable devices and energy capacity in the conventional Li-ion system might increase in the near future.[1] Therefore, intensive research efforts are still necessary to enhance the properties of Li-ion system. Therefore, much research has been actively pursued to improve the electrochemical properties of Li-ion batteries components such as anode, cathode, separator as well as electrolyte.

For the case of anode material, despite of excellent capacity

retention of graphite electrode, it is not suitable for advanced Li-ion systems due to its low specific capacity and poor rate capability.[3,14,17] Numerous materials have been proposed for candidates replacing the graphite such as Li alloying materials (Group Ⅳ and Ⅴ elements)[13,18-39] and intercalation materials.[3,40,41] Most of all, Si based systems are definitely attractive candidates since Si has a large theoretical specific capacity at room temperature ($Li_{15}Si_4$: 3600 mAh g^{-1}) and low operating voltage (near 0.1 V vs. Li/Li^+).[42,43] However, in general, most Si based electrodes have some problems to apply for anode material because of its large volume change during cycling and a poor rate capability.[1,13] The stress induced by a large volume change during the cycling cause pulverization of Si which leads to loss of electrical contact with current collector and formation of solid electrolyte interphase (SEI) layer on the electrode surface repetitively.[39]

To alleviate these problems, formation of the core-shell structure[44-46] and using nano-materials[21,46,47] was employed in this study. Using of nano-material can efficiently accommodate the volume changes. In core-shell structured materials, the electronic conducting and structural stable shell not only buffers volume expansion of Si particles during cycling but

also acts as an electrical conducting pathway.[23] The core-shell nanocomposites were developed with a homogeneous coating of second material on Si such as conducting carbon, surface oxide and metal, recently.[48-50]

One of the effective approaches for formation of core-shell structure is the design of carbon coated nanostructure with nano-thickness improve the electrochemical properties of Si-based electrodes.[51-54]. Recently, various carbon coating techniques have been suggested such as hydrothermal, high energy mechanical milling (HEMM) and chemical vapor deposition (CVD). Among various carbon coating techniques, substrate induced coagulation (SIC) method was very efficient tool to prepare a large amount of core-shell structured materials at one time.[53,54] This method has been widely used for coating carbon nano-layer on any type of surface.[53,54] Meanwhile, for the carbon coating, poly vinyl alcohol (PVA) was chosen. Generally, PVA has been used in SIC process and widely applied to modify the electrode material as well since PVA can be dissolved easily in distilled water and transformed to carbon black by simple carbonization process. With SIC method, a large amount of nano-Si/C core-shell structured material could be simply prepared.

On the other hands, SnO_2, which is chosen for shell material, is one of the most promising systems as an anode material for LiBs.[55-58] Basically, the reaction mechanism of SnO_2 with Li can be expressed as follows:[13,59]

$$SnO_2 + 4Li + 4e^- \rightarrow Sn + 2Li_2O \quad (1.1)$$

$$4.4Li^+ + Sn + 4.4e^- \leftrightarrow Li_{4.4}Sn \quad (1.2)$$

Li_2O can act as a buffering matrix against volume change and suppress the agglomeration of Sn particles during cycling.[13] Recently, it was reported that SnO_2 electrodes showed a higher reversible capacity than the theoretical reversible capacity calculated for the above reaction mechanism (SnO_2 electrode, $Li_{22}Sn_5$: 781 mAh g^{-1}).[28,56-58] However, most reports did not clearly explain the phenomenon of higher capacity. Lian et al.[56] and Lou et al.[57] suggested that this phenomenon could be caused by the partial recombination of SnO_2. By combining Si and SnO_2, the aforementioned advantages of these materials can be utilized fully in the anodes of LiBs.

In this works, nano-Si/C and nano-Si/SnO_2 core-shell nanostructured material were synthesized by a simple SIC methods and sol-gel method, respectively. These core-shell nanostructured electrodes showed much better electrochemical properties than nano-Si electrode. And also reaction

mechanism of each electrode was confirmed by various analyses such as *ex situ* XRD and TEM analyses. In case of a nano-Si/SnO_2 core-shell nanostructured electrode, the partial reversibility of SnO_2 during the first cycle was identified by TEM analysis. On the basis of their excellent electrochemical properties, these core-shell nanostructured electrodes could be a strong candidate as anode materials for LiBs.

Chapter 2. Theoretical Background

2.1 Fundamental of Rechargeable Li-ion Batteries

2.1.1 History

A battery is a device which converts stored chemical energy into electrical energy by oxidation/reduction reaction of electrode. Basically, a battery is made up of 4 components such as cathode, anode, separator and electrolyte. When the cell is charged (or discharged), redox reaction occurs between the electrode surface and electrolyte while electrolyte functions as a Li ion conductor and separator prevents the circuit shortage. Historically, the term ‘battery' was coined by Benjamin Franklin to describe multiple charged glass plates in 1748. But, the term has evolved to include a single cell in these days. In 1791, Luigi Galvani's experiment with a frog, which was consisted of two different metals, was similar as the circuit. About the same time, Alexandria Volta, a professor of physics in Pavia, repeated and checked Galvani’s experiments. Volta started his work to doubt the Galvani's results and he suggested that the current was generated by making a contact between two different metals instead of 'animal electricity'. And then, he invented the Volta battery which is the first

primary battery in history. In 1836, John Frederic Daniell invented technically improved Daniell cell consisted of a copper pot filled with a copper sulfate solution, in which was immersed an unglazed earthenware container filled with sulfuric acid and a zinc electrode. Thereafter, Grove cell, Bunsen cell, Poggendorf cell and Lechlanche cell were also designed and batteries have become a common energy source for many applications. The history of batteries is summarized in Table 1.[61]

Li ion batteries (LiBs) are one of the most promising system, which are used widely in various electronic devices. LiBs have many advantages such as high power, large reversible capacity and no memory effect. Presently, conventional LiBs employ a carbonaceous material for anode material and $LiCoO_2$ for cathode material. In 1970s, M. S. Whittingham propose the LiBs, consisting of titanium sulfide as cathode and Li metal as anode, for the first time.[60] And then a lot of researches were performed to improve performances of LiBs. Through many trials and errors, Bell labs developed a graphite anode, which shows an excellent capacity retention during the cycling, to provide a replacement for Li metal anode.[62] Following the breakthrough, the first commercialized LiBs was developed by Sony.[7]

2.1.2 Principle

Electrode materials of first commercialized Li-ion battery consist of graphite for anode material and $LiCoO_2$ for cathode material, respectively. Figure 1 illustrates the basic concept of Li-ion batteries. When an external electrical energy is provided into the cell, Li ions are extracted from the $LiCoO_2$ electrode and transferred to the graphite electrode through the non-aqueous electrolyte (charge process). In discharge process, which the situations changed in reverse, Li-ion battery can be utilized for the energy source. The reaction mechanism of commercial Li-ion batteries are as follows :

Graphite electrode : $C_n + xLi^+ + xe^- \leftrightarrow C_nLi_x$ (2.1)

$LiCoO_2$ electrode : $LiCoO_2 \leftrightarrow Li_{1-x}CoO_2 + xLi^+ + xe^-$ (2.2)

Total : $LiCoO_2 + C_n \leftrightarrow Li_{1-x}CoO_2 + C_nLi_x$ (2.3)

2.1.3 Terminology

i) ***Operating voltage*** : One of the important parameter of a battery system is the operating voltage at which it operates during discharge- when it supplies electrical energy and power- and when it is being recharged. The open circuit voltage is determined by thermodynamic of electrochemical half reactions between each electrodes. During actual use, however, the

Table 1. The history of Batteries

Year	System	Inventor
1791	Galvani's experiment with a frog leg	Gavani
1800	$Cu/H_2SO_4/Zn$	Volta
1813	Giant battery	Davy
1836	$Cu/CuSO_4/ZnSO_4/Zn$	Daniell
1839	Priniple of the air cell	Grove
1859	$PbO_2/H_2SO_4/Pb$	Plante
1868	$Zn/NH_4Cl/C$ wet battery	Leclanche
1875	Edison's first battery patent (MnO_2 battery)	Edison
1881	Pb-Sb alloy	Sellow
1885	Zn/Br_2 battery	Bradly
1905	Ni/Fe battery	Edison
1927	Zn/Ag battery	Andre
1930	Ni/Zn battery	Drumm
1935	Pb-Ca alloy (fro Lead-Acid battery)	Haring & Thomas
1950	Hermetic Zn/HgO battery	Ruben
1956	Alkaline Fuel cell	Bacon
1966	Na/S battery	Kummer & Weber
1970	Primary Li battery	Tobias
1980s	Practical use of Li/MnO_2 battery	Moli
1990s	Reusable alkaline commercial Li-ion battery	Kordesch Sony

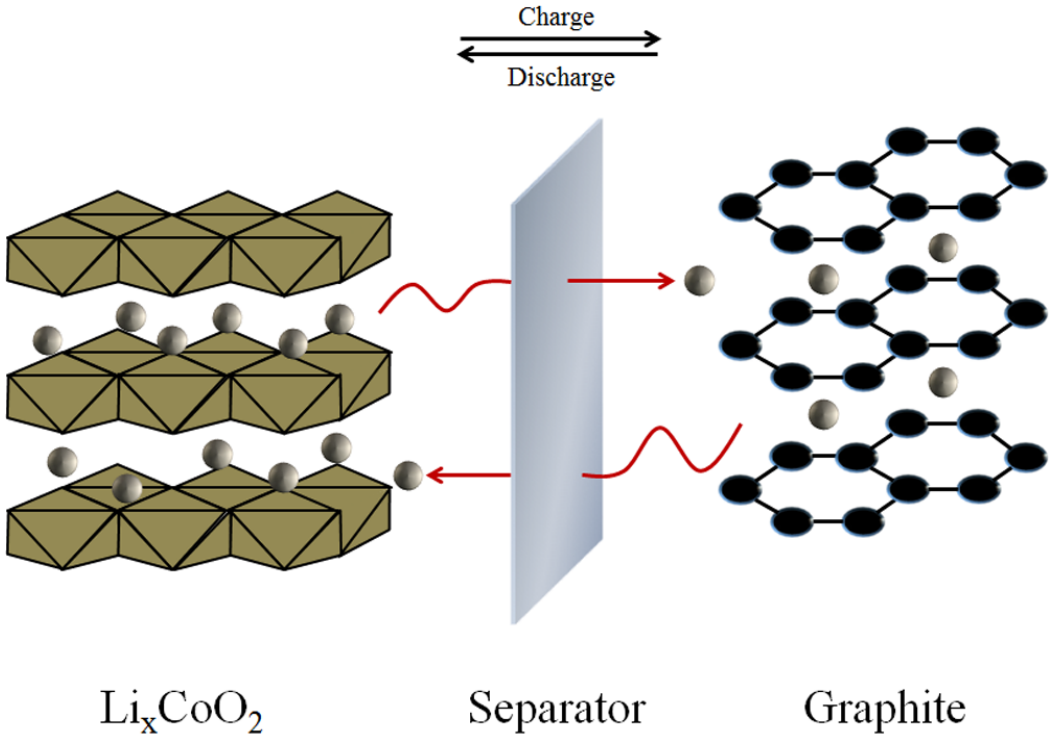

Figure 1. The principle of operation of the first commercialized Li-ion batteries.

operating voltage will vary from these thermodynamic values, depending on various kinetic factors.[9]

ii) ***The charge capacity*** : The meaning of charge capacity is the amount of charge that can be supplied to the external circuit from an electrochemical system.

iii) ***The maximum theoretical specific capacity*** : Faraday's law explains that the mass of anodic material of a galvanic cell depends on the current I passing by the system according to[63] :

$$m = -\frac{MI\delta t}{xF} \tag{2.4}$$

Where m is the mass of active, M is the molar mass, x is the number of electron exchanged, δt is the elapsed time, and F is the Faraday's constant. The capacity of a cell, Q is given by :

$$Q = I\delta t \tag{2.5}$$

Therefore, Eq (2.4) can be rearranged :

$$Q_m = \frac{I\delta t}{m} = \frac{xF}{M} \tag{2.6}$$

With Q_m the gravimetric capacity. And Q_m multiplied by the density (d) of

the active material, becomes :

$$Q_v = Q_m \times d \tag{2.7}$$

Where Q_v is the volumetric capacity.

iv) ***Initial Coulombic efficiency*** : Among the electrochemical properties of electrode, especially anode materials, initial Coulombic efficiency is the important factor due to the limited amount of Li ion in the full cell batteries. Initial Coulombic efficiency can be expressed as follows :

$$ICE = \frac{Q_c}{Q_d} \tag{2.8}$$

Where Q_c is the first cycle discharge capacity (lithiation process) and Q_d is the first cycle charge capacity (delithiattion process).

v) ***Cyclabiltiy*** : The capacity of the battery decreases during cycling. Generally, cyclabiltiy is defined as the capacity of the battery goes down to the 60 % of initial capacity.

vi) ***Rate capability*** : Base on the electrode has a good cyclabiltiy, rate capability is other parameters to evaluate the electrochemical properties of electrode. Commonly, 'C-rate' concept is used for comparison of this

performance. In general, 1 C is the rate to charge or th discharge the electrode in an hour. If a battery shows similar capacity at various C rates, it can be said that this battery has an superior rate capability.

vii) ***Self discharge*** : Self discharge implies a decrease in available capacity with time, even without energy being taken from the cell by the passage of current through the external circuit.[9]

2.2 Components of Rechargeable Li-ion Batteries

2.2.1 Anode

The early days of rechargeable Li ion batteries, metallic Li was used as anode materials because of its high theoretical capacity (3860 mAh g^{-1}) and low operating potential. Despite of these advantages, metallic Li anode had some problems such as the periodic dissolution and deposition of metallic Li during cycling. These problem should be solved for using Li metal as anode materials. After several years, Bell labs developed a graphite anode to replace the metallic Li anodes. Graphite anode, by contrast, does not suffer from periodic dissolution and deposition problem during cycling, shows an excellent capacity retention and has a low

operating voltage.[62] Besides graphite, many other carbonaceous material can be used as anode material such as amorphous carbon, carbon nanotube (CNT) and graphene. Commonly, carbons that are capable of reversible Li ion batteries can roughly be classified as "graphitic" and "non-graphitic".[3,64] Graphitic carbons are carbonaceous materials with a layered structure but typically with a number of structural defects. Non-graphitic carbonaceous materials consist of carbon atoms that are mainly arranged in a planar hexagonal network but without far-reaching crystallographic order in the c-direction and they can be further classified into soft and hard carbon.[3] These carbonaceous materials has its own electrochemical properties depending on the crystal structure, surface condition and particle size. However, carbonaceous anodes, especially graphite anodes have a small reversible capacity (LiC_6 : 372 mAh g^{-1}) and a poor rate capability, so it is not suitable for the new large units applications.[13,14,17]

There are many candidates to replace carbonaceous anode such as Li alloying materials (Group Ⅳ and Ⅴ elements)[13,18-39] and intercalation materials.[3,40,41] Theoretical capacity of various Li-M alloys are given in Table 2. In case of single elements system, Si, Sn, Ge, P, As, Sb, Bi, Pd,

Cd etc. can be used for anode material as shown the following reaction.

$$Li_xM \leftrightarrow xLi^+ + xe^- + M \quad (2.9)$$

Because of high energy density of alloy based material, a lot of researches have been conducted as alternatives to graphite. Alloy based material electrodes, however, have serious problem. During cycling those electrodes experience severe volume change, which has a bad influence on battery life. To alleviate the volume expansion of electrode, various attempts have been conducted such as using nanomaterials,[29,46,47] unique nanostructures,[19,39,44-46] mixing composite with carbon[65-67] and active-inactive material composite concepts.[65-67] On the other hands, Li can alloy with intermetallic compounds by conversion reaction (Eq. 2.10) or insertion reaction (Eq. 2.11). Each reactions can be expressed as follows :

$$AB + xLi^+ + xe^- \leftrightarrow Li_xA + B \quad (2.10)$$

$$AB + xLi^+ + xe^- \leftrightarrow Li_xAB \quad (2.11)$$

In case of conversion reaction, decomposed element B can act as buffering matrix against the volume change during cycling.[68-71] On another occasion, insertion reaction, Li based ternary intermetallic phase are formed

after lithiation process.[72-75]

2.2.2 Cathode

Currently, various layered structure materials have been proposed as cathode material for LiBs such as inorganic transition metal oxides and chalcogenides. Their basic reaction equation with Li is as follows :[3]

$$\Delta x\, Li^{+} + \Delta x e^{-} + Li_{x}MX \underset{charge}{\overset{discharge}{\rightleftharpoons}} Li_{x+\Delta x}MX \qquad (2.12)$$

Where X is transition metal oxides or chalcogenides; $x \geq 0$. Their specific charges are based on a reversible range Δx of the Li content during the cycling. These materials show stable cyclabilities, however, its capacity is only 130 ~ 140 mAh g^{-1} which is smaller capacity than that of graphite electrode. And some cathode materials have safety issues due to the overcharge of cell. For these reasons, the intensive efforts to enhance the electrochemical properties are necessary. Representative cathode materials and their characteristics are shown in Table. 3.[3] Cathode materials that contain no Li after their synthesis are in the charged state.

2.2.3 Electrolyte

The main role of electrolyte is the path for the ion movement between anode and cathode. There are two kinds of electrolytes such as the liquid state electrolyte and the solid state electrolyte. The common electrolytes are liquid type that consists of salts dissolved in solvent due to their superior ionic conductivity at ambient temperature. Generally, electrolytes for LiBs have to satisfy the following requirements such as good ionic conductivity ($>10^{-3}$ S cm^{-1} from - 40 ^{o}C to 90 ^{o}C), Li ion transference number approaching unity, wide electrochemical voltage window (0 ~ 5 V vs. Li/Li^{+}), Thermal stability (up to 90 ^{o}C) and compatibility with other cell components.[2,8,76] Ideal solvent of electrolyte should satisfy the following requirements : [76]

i) Aprotic, high polarity and lower viscosity

ii) Lower melting point a wide temperature range

iii) higher boiling point a lower vapor pressure

iv) Molecular structure, inter-molecular force

v) Higher dielectric constant

Lithium salts in the electrolyte solutions act as charge carriers during

cycling. Good solubility and charge separation are the basic requirements of good Lithium salt. Table. 4. shows the characteristics of various solvent and salts[76] and figure 2 shows the chemical structures of solvent and co-solvent as electrolytes for LiBs.

2.3 Silicon

Silicon is the member of the group Ⅳ elements in the periodic table with the symbol Si, atmoic number 14 and atomic weight 28.085. Silicon was first prepared and characterized in pure form in 1824 and suggested its english name in 1831. Silicon is the eight most common element in the universe by mass and the most amount of silicon is buried as a form of oxides and silicates.[77]

Silicon is a solid state at room temperature, with relatively high melting temperature of approximately 1414 ^{o}C. Interestingly, silicon doe not contract when it freezes because silicon has a greater density in a liquid state (2.57 g cm^{-3} at melting temperature) than a solid state (2.33 g cm^{-3} at room temperature) similar to how ice is less dense than water. Typically, pure silicon has a diamond cubic crystal structure (a ≈ 0.543 nm), a gray

Table 2. Maximum theoretical capacity of various Li-M alloys.

Element (M)	Li-M alloy phase	Theoretical capacity (mAh g^{-1})
C	LiC_6	372
Si	$Li_{22}Si_5$	4198
Ge	$Li_{22}Ge_5$	1620
Sn	$Li_{22}Sn_5$	993
Pb	$Li_{22}Pb_5$	569
P	Li_3P	2596
As	Li_3As	1074
Sb	Li_3Sb	660
Bi	Li_3Bi	385
Al	Li_9Al_4	2235
Ga	Li_2Ga	769
In	$Li_{13}In_3$	1012
Mg	$Li_{11}Mg_3$	4077
Ag	Li_4Ag	994
Zn	LiZn	410
Cd	Li_3Cd	715
S	Li_2S	1672

Table 3. Characteristics of representative cathode materials for LiBs

Material	Molecular weight	Density [kg/L]	Reversible Range Δx	Theoretical specific charge [Ah/kg]	Theoretical charge density [Ah/L]
Charged					
TiS_2	112.01	3.27	1	239	782
MoS_2	160.06	5.06	0.8	134	678
V_2O_5	181.88	3.36	1	147	495
V_6O_{13}	513.64	3.91	3.6	188	734
MnO_2	86.94	5.03	0.5	154	775
$NbSe_3$	329.81	8.7	3	244	2121
Discharged					
$LiCoO_2$	97.87	5.16	0.5	137	706
$LiNiO_2$	97.63	4.78	0.7	192	919
$LiMn_2O_4$	180.82	4.28	1	148	634

Table 4. The characteristics of various solvent and salts as electrolyte for LiBs.

Electrolytes	Characteristics
Solvent	
EC	High melting temperature
PC	graphite exfoliation
Co-solvent	
DEC	Low melting temperature, high viscosity
DMC	High melting temperature, low viscosity
EMC	Low melting temperature, low viscosity
Salt	
$LiPF_6$	High ionic conductivity
$LiBF_6$	Safety
$LiAsF_6$	excellent properties (but toxic)
$LiClO_4$	Safety problems
$LiN(SO_2CF_2CF_3)_2$	Corrosion of Al foil
$LiCF_3SO_3$	Low ionic conductivity

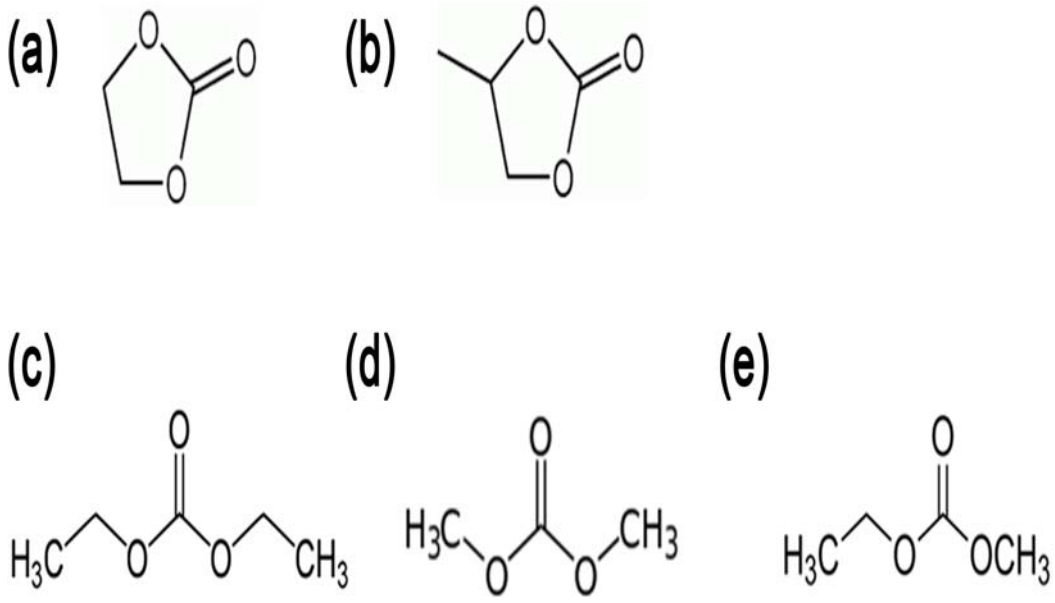

Figure 2. Chemical structures of solvent, (a) EC, (b) PC and co-solvent (c) DEC, (d) DMC, and (e) EMC as electrolyte for LiBs.

color and a metallic luster. Like germanium, silicon is rather strong, very brittle and prone to chipping.[78] It is well known that the silicon is a representative semiconductor material. The outer electron orbital of silicon has four valence electrons. The 1s, 2s, 2p and 3s subshells are fully filled while the 3p subshell contains two electrons. Single crystal silicon wafer has wide usage as semiconductor in the industry-wide.

For LiBs anode material, silicon is the one of the most attractive materials due to its large theoretical specific capacity at room temperature ($Li_{15}Si_4$: 3600 mAh g^{-1}) and low operating voltage (near 0.1 V vs. Li/Li^+).[42,43] The reaction mechanism of Si electrode is as follows :[13]

During lithiation

$$Si + xLi^+ + xe^-$$

$$\rightarrow Li_xSi \text{ (amorphous)} + (3.75\text{-}x)Li^+ + (3.75\text{-}x)e^- \quad (2.13)$$

$$\rightarrow Li_{15}Si_4 \text{ (crystalline)} \quad (2.14)$$

During delithiation

$$Li_{15}Si_4 \text{ (crystalline)}$$

$$\rightarrow Si \text{ (amorphous)} + yLi^+ + ye^- + Li_{15}Si_4 \text{ (residual)} \quad (2.15)$$

In the two phase resion, crystalline Si becomes an amorphous Li-Si alloy (2.13) and the amorphous phase suddenly crystallizes as a $Li_{15}Si_4$ phase around 50 mV (vs. Li/Li^+). After the delithiation process, Si becomes amorphous phase.[13] Due to electrical disconnection of the active material caused by a severe volume change, there are some amounts of the residual $Li_{15}Si_4$ phase. after the first delithiation, which results in a large irreversible capacity.[13] Despite the advantage of Si electrode, in general, most Si based electrodes have some problems such as a large volume change during cycling and a poor rate capability.[1,13] The stress induced by a large volume change during the cycling cause pulverization of Si which leads to loss of electrical contact with current collector and formation of solid electrolyte interphase (SEI) layer on the electrode surface repetitively.[39] To alleviate these problems, various Si-based systems have been proposed, such as Si-M alloy,[79-82] Si-based composite,[65,66,83-87] Si oxide[30,88-97] and unique nanostructured Si materials.[21,98-100]

2.4 Core-shell Nanostructured Materials

Nowadays, design of nanostructured materials are one of the main issues as

alternative anode materials. Basically, nanomaterials has many advantages such as high capacity due to their high interfacial area, high rate capabililty by reducing Li ion diffusion path and stable cycling behavior by accommodating the strain generated during the cycling. Among the unique nanostructure, core-shell structure is one of the most promising structure as electrode materials for LiBs.[101]

Core-shell structure consists of inner core materials surrounded by other materials as shell, which source from a traditional concept of the semiconductor field. Generally, the core material is the main component for electrode, while the shell material acts as a protection layer to keep the core electrochemical performance or to give new properties. And shell materials prevent the sensitively active cores from directly contacting the electrolyte and then avoiding or restricting the unnecessary side reactions. The poor electrical conductivity or large volume change during cycling of core material could overcome by this structure. To enhance electrical conductivity, highly conductive materials are suitable for shell materials such as carbon material,[101-104] metal oxide,[101,105-108] electrically conductive polymers. To accommodate the volume expansion, structural stable acitve

material during the cycling or inactive materials are suitable such as amorphous carbon,[101-104] graphene,[109-114] metal oxides,[115-118] and are better when they are filled with pores. Therefore, well combined core-shell structured materials often shows excellent electrochemical properties over their single component because of above reasons.

Chapter 3. Experimental

3.1 Electrode Preparation

3.1.1 Active Materials preparation

nano-Si/C core-shell nanostructured material : Among various carbon coating techniques, substrate induced coagulation (SIC) method[119-120] was used to prepare a nano-Si/C core-shell nanostructured material. For the preparation of nano-Si/C core-shell nanostructure, 0.2 wt.% of PVA (Sigma-Aldrich, 99+ %, hydrolyzed) was dissolved in distilled water at 60 ^{o}C with stirring and the solution was cooled down to room temperature. Si nano-powders (Aldrich, nano-powder, <100 nm) were put into PVA solution and stirred for 5 min. This nano-Si/PVA solution passed through centrifuge process for 5 times at 4500 rpm for 10 min, and dried in vacuum oven at 60 ^{o}C for 24 h. For the carbonization of PVA, dried nano-Si/PVA was calcined at 750 ◦C for 3 h under Ar atmosphere to obtain core-shell structured nano-Si/C. Carbonization temperature was determined based on the result of thermo-gravimetric analysis (TGA) of PVA since no weight loss was observed above 500 ◦C. Preliminary studies showed that the above

condition was an optimum for better electrochemical behaviours. For comparison, micron-size Si/C core-shell structured material was also prepared using the same method with micron size Si powder (Kosundo, 99%, 4 μm).

nano-Si/SnO_2 core-shell nanostructured material : The nano-Si/SnO_2 core-shell nanostructured material was prepared as follows. Commercial nano-Si particles (0.075 g, Aldrich, <100nm) was put into distilled water (50 mL) with sonification for dispersion. Potassium stannate trihydrate (0.5 g, $K_2SnO_3 \cdot 3H_2O$, Sigma-Aldrich) was dissolved into prepared nano-Si solution with stirring for 10min, followed by the addition of absolute ethanol (25 mL). The solution was heated to 60 °C for 1 h with mild stirring. The product was washed, collected by centrifuge and dried in a vacuum oven at 90 °C. SnO_2 hollow spheres were synthesized by sol-gel method using an SiO_2 template, in order to compare the cyclability with the nano-Si/SnO_2 core-shell nanostructured material. The procedure is described in detail else where.[28]

3.1.2 Electrode and Cell Assembly

nano-Si/C core-shell nanostructured electrode : The test electrodes consisted of the active powder material (70 wt.%), carbon black (Ketjen Black, 15 wt.%) as a conducting agent and poly amide imide (PAI, 15 wt.%) dissolved in N-methyl pyrrolidinone (NMP) at 60 ^{o}C as a binder. Each component was well mixed to form a slurry using a magnetic stirrer. That slurry was coated on a copper foil substrate, pressed, and dried at 200 ^{o}C or 4 h under a vacuum. A coin-type, laboratory-made electrochemical cell was used with lithium foil as the counter and reference electrode and 1 M $LiPF_6$ and 10% fluoroethylene carbonate (FEC) in ethylene carbonate (EC)/diethyl carbonate (DEC) (3:7 (v/v), PANAX) as the electrolyte. The cell assembly and all of the electrochemical tests were carried out in an Ar-filled glove box using Celgard 2400 as a separator.

nano-Si/SnO_2 core-shell nanostructured electrode : The test electrodes consisted of the active powder material (70 wt.%), carbon black (Ketjen Black, 10 wt.%) as a conducting agent, and PAI (20 wt.%) dissolved in NMP at 60 °C as a binder. Each component was well mixed to form a slurry using a magnetic stirrer. The slurry was coated onto a copper foil substrate, pressed, and dried at 200 °C for 4 h under vacuum.

A coin-type, laboratory-made electrochemical cell was used with Li foil as the counter and reference electrodes, and $LiPF_6$ (1 M) and FEC (10 %) in EC / DEC (3 : 7 (v/v), PANAX) were used as the electrolyte. The cell assembly and all of the electrochemical tests were carried out in an Ar-filled glove box using Celgard 2400 as a separator.

3.2 Electrochemical Test

3.2.1 Galvanostatic Test

nano-Si/C core-shell nanostructured electrode : The cell experiments were galvanostatically performed using a Maccor automater tester at a constant current of 100 mA g^{-1} (100 mA g^{-1}, 300 mA g^{-1}, 500 mA g^{-1}, 1000 mA g^{-1}, 1500 mA g^{-1}, 100 mA g^{-1} at each step in the rate capability test) for the active material within the voltage range between 0.0 V and 1.5 V (vs. Li/Li^+). During the discharging step, Li was inserted into the electrode, while Li was extracted from the electrode during the charge.

nano-Si/SnO_2 core-shell nanostructured electrode : The cycling experiments were galvanostatically performed using a Maccor automated

tester at a constant current of 200 mA g^{-1} (100 mA g^{-1}, 200 mA g^{-1}, 500 mA g^{-1}, 1000 mA g^{-1}, 1500 mA g^{-1}, 100 mA g^{-1} at each step in the rate capability test) for the active material within the voltage range between 0.0 V and 2.5 V (vs. Li/Li^{+}). During the discharging step, Li was inserted into the electrode, while Li was extracted from the electrode during the charge.

3.2.2 Differential Capacity Plot (DCP)

DCP can be obtained by differential from the discharge/charge plot. DCP provides an information about both the reaction characteristics and performance of electrode, and this is similar as that of cyclic voltammetry (CV) curve. In this plot, voltage plateaus in charge-discharge plot can be expressed as each peaks.

$$\frac{dQ}{dV} = \frac{I[t(n+1)-t(n)]}{m[V(n+1)-V(n)]} \qquad (2.13)$$

Where t(n+1) and t(n) are the time of selective point, V(n+1) and V(n) are the voltage of selective point and m is the mass of active material.

3.3 Material Characterization

3.3.1 X-ray Diffraction (XRD)

Fundamental : XRD analysis is a non-destructive analytical technique which reveals the crystal structure of samples. The XRD pattern represents characteristic of materials like a fingerprint. This XRD analysis is based on the Scherrer equation which was published by P. Scherrer in 1981.[121] Scherrer equation can be expressed as follows :

$$\tau = \frac{K\lambda}{\beta\cos\theta} \qquad (3.1)$$

Where β is the line broadening at galf the maximum intensity (FWHM), K is the shape factor, λ is the x-ray wavelength and Θ is the Bragg angle; τ is the mean size of the ordered domains which may be smaller or equal to the grain size. From the XRD patterns of the samples, a lot of informations about the samples can be obtained such as phase, crystal structure, solid solution residual stress, texture and average crystallite size. Schematic image about principle of XRD is shown in figure 3.[122]

Experimental : Samples were characterized using an X-ray diffractometer (XRD, Rigaku, D-MAX2500-PC) with Cu-Kα radiation. Conditions for XRD analysis were acceleration voltage 40 kV, current 100 mA, sampling width 0.02 mm and scanning rate 10 degree/minute. *Ex situ* XRD was used to observe the structural changes occurring in the active

material during cycling. To prepare the XRD samples, the electrodes were detached from the coin-type electrochemical cell, washed with DEC, dried for 3 h in an Ar-filled glove box, and coated with Kapton tape, which served as a protective film.

3.3.2 Scanning Electron Microscope (SEM)

Fundamental : A SEM is a one of electron microscope that produces images by scanning a sample with a high energy (typically 10 keV) electron beam. The incident electrons interact with electrons in the sample, producing various signals that can be detected. Among the signals, low energy secondary electrons, escaped from the sample surface are detected by attracting them onto a phosphor screen and from this signal, information about the sample's surface topography and composition can be obtained. On the other hands, the incident electrons will also cause x-ray and that signal is the basis of the energy dispersive spectroscopy (EDS) technique. Schematic image about principle of SEM is shown in figure 4.[123]

Experimental : the morphology of samples was observed using field emission scanning electron microscope (FESEM, Carl Zeiss, SUPRA

55VP). Nano-Si/SnO_2 core-shell nanostructured material was identified with electron dispersive spectroscopy (EDS, Hitachi, SU70). Small amount of samples were loaded on a holder previously covered with carbon tape.

3.3.3 Transmission Electron Microscope (TEM)

Fundamental : The basic principle of TEM is same as the light microscope but uses electrons instead of light. The wave length of electrons is much lower than that of light and it make possible to get a resolution a thousand times better than with a light microscope. The sample of TEM have to be prepared ultra thin to facilitate the transmission of electron through sample. Schematic image about principle of XRD is shown in figure 5.[123]

Experimental : The samples were identified with the high resolution transmission electron microscope (HRTEM, JEOL, JEM-3000F) with EDS mapping (FEI, Tecnai F20). For HRTEM analyses, the dilute suspensions of the samples were placed on a carbon-coated grid. All HRTEM sample preparation processes were conducted in an Ar atmosphere glove box. To identify the final Li-Si binary phase when the electrode was fully lithiated, an electrode (lithiated to 0.0 V) was detached from the Cu substrate,

washed with DEC, put into an alumina crucible, and sealed. This sealed sample was heat-treated at 500 °C for 12 h in an Ar atmosphere at a heating rate of 5 °C min^{-1}. After heat treatment, the furnace was cooled automatically to room temperature.

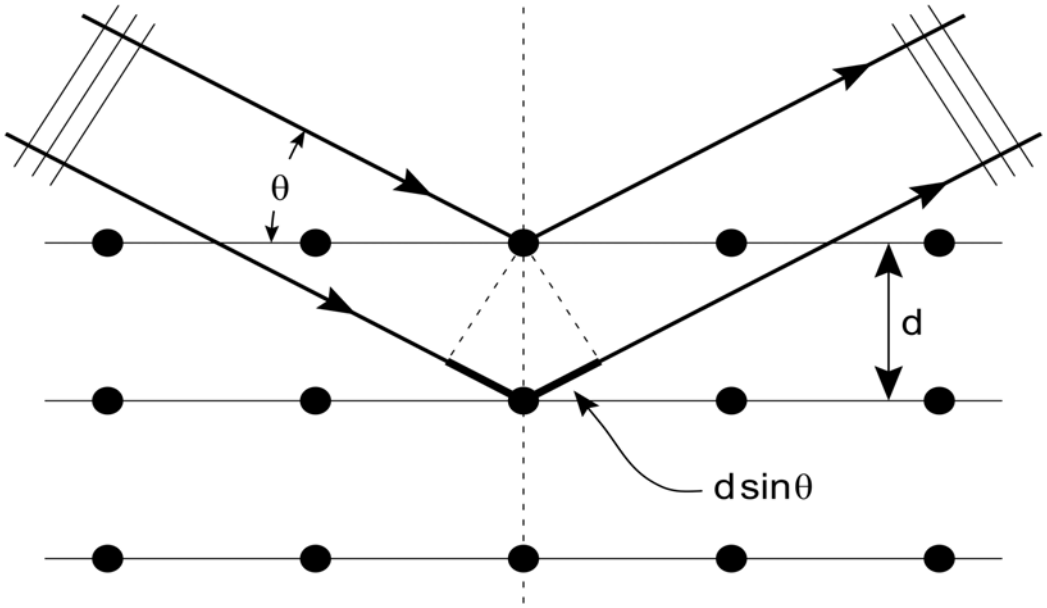

Figure 3. Schematic illustration of principles of XRD.

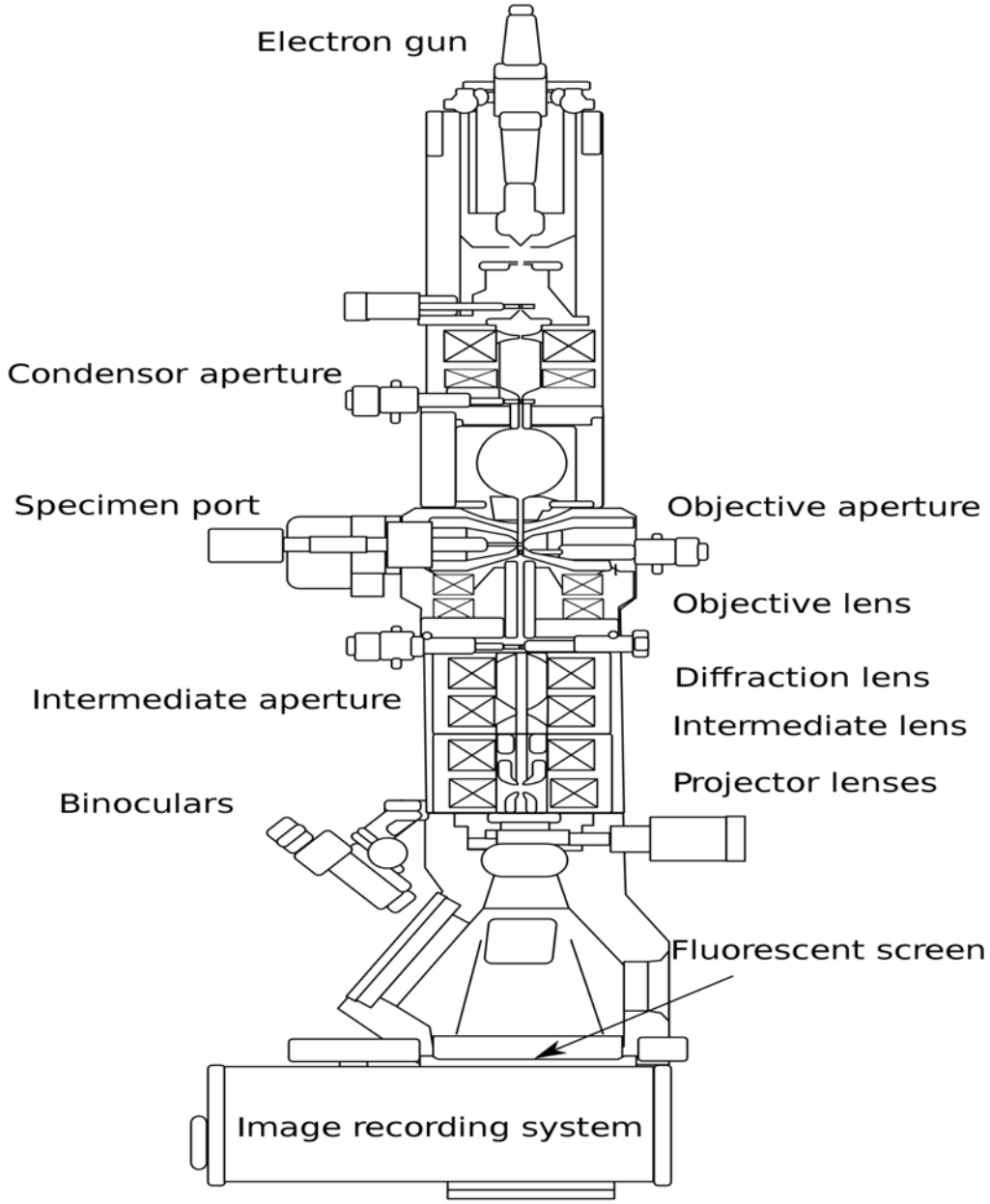

Figure 4. Schematic illustration of principles of SEM.

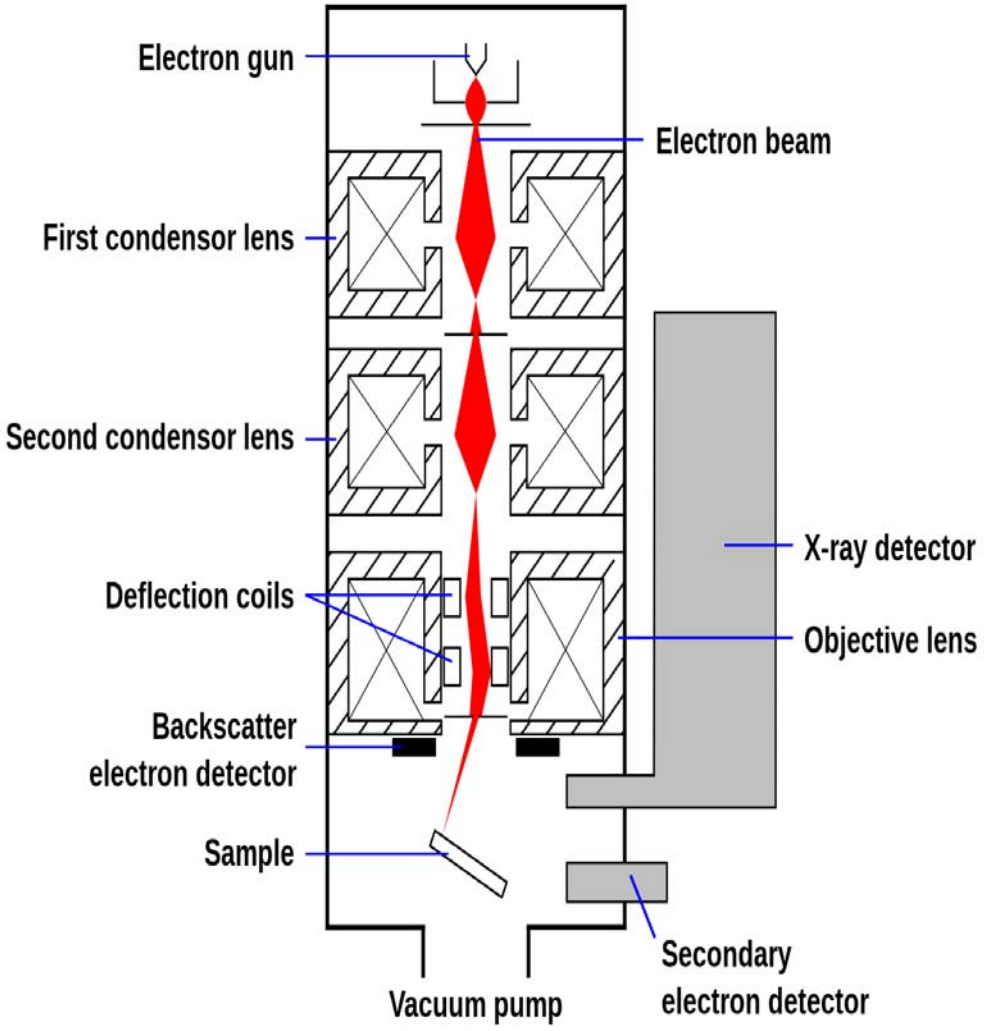

Figure 5. Schematic illustration of principles of TEM.

Chapter 4. Results and Discussion

4.1 nano-Si/C Core-shell Material

4.1.1 Material Characterization

XRD patterns of nano-Si, nano-Si/PVA and nano-Si/C core-shell nanostructured material are shown in figure 6. The XRD peaks of Si were observed and there was no change for XRD patterns after coating PVA and carbonization. The average crystallite size of Si in each sample was estimated using Scherrer's equation, and 21.2 nm for nano-Si, 25.5 nm for nano-Si/PVA and 29.2 nm for nano-Si/C. FESEM image of nano-Si/C showed that nano-Si/C particles were partially agglomerated in figure 7. Figure 8a is the schematic illustration on the morphology concept of nano-Si/C core-shell nanostructured material. Each nano-Si particle core was coated with amorphous carbon shell and amorphous carbon shell was connected to adjacent amorphous carbon shell. This concept was confirmed by HRTEM image (figure 8b). Corresponding to schematic illustration, the shape of nano-Si/C core-shell nanostructured material particles looks like frog spawn and connected in series with each other continuously.

Figure 9a and b are HRTEM images of nano-Si/PVA (as coated),

while figure 10a and b are HRTEM images of nano-Si/C core-shell nanostructured material images (after carbonization), and the size of Si crystallites was comparable to that of estimated size from the XRD data. Before carbonization, crystalline nano-Si was coated with PVA layer of 5 – 10 nm thickness uniformly (figure 9b). After the carbonization, PVA layer was transformed to the amorphous carbon layer (figure 10b). The thickness of coating layer, about 5 - 10 nm thickness, was not significantly changed during carbonization. These results demonstrated that the morphology concept of nano-Si/C was engineered to obtain the frog spawn shape core-shell structure with amorphous carbon shell of 5 – 10 nm thickness.

4.1.2 Electrochemical Characterization

The voltage profiles of nano-Si/PVA electrode and nano-Si/C core-shell nanostructured electrode are shown in figure 11. There was a huge difference of the first cycle capacity between nano-Si/PVA electrode and nano-Si/C core-shell nanostructured electrode. The capacity difference between these two electrodes was caused mainly by the difference of electrical conductivity of the coated materials[125], and confirmed in this study that the conductivity of nano-Si/C was two orders of magnitude

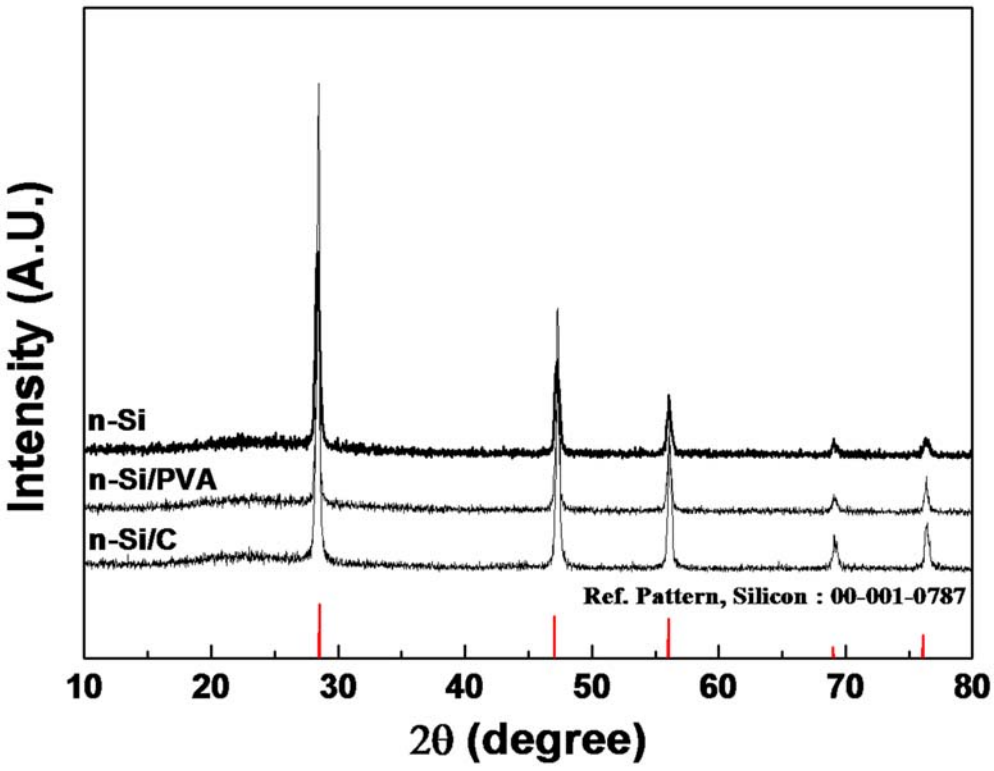

Figure 6. X-ray diffraction patterns of various electrodes samples.

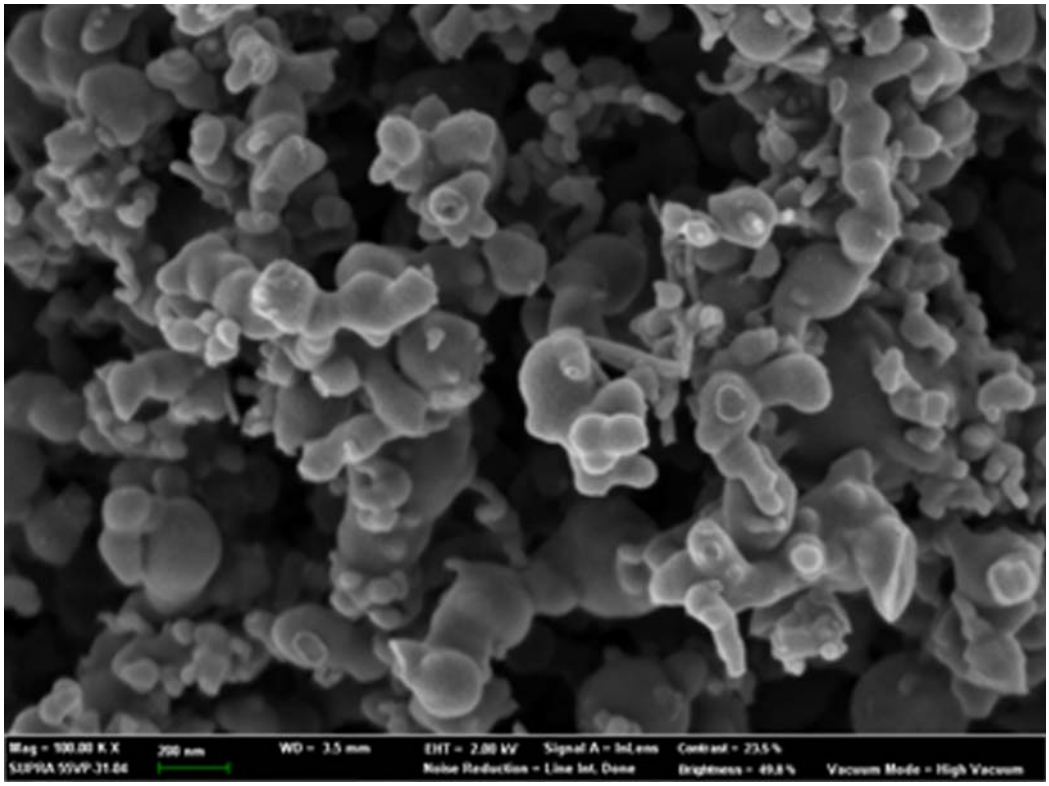

Figure 7. FESEM image of nano-Si/C core-shell nanostructured material.

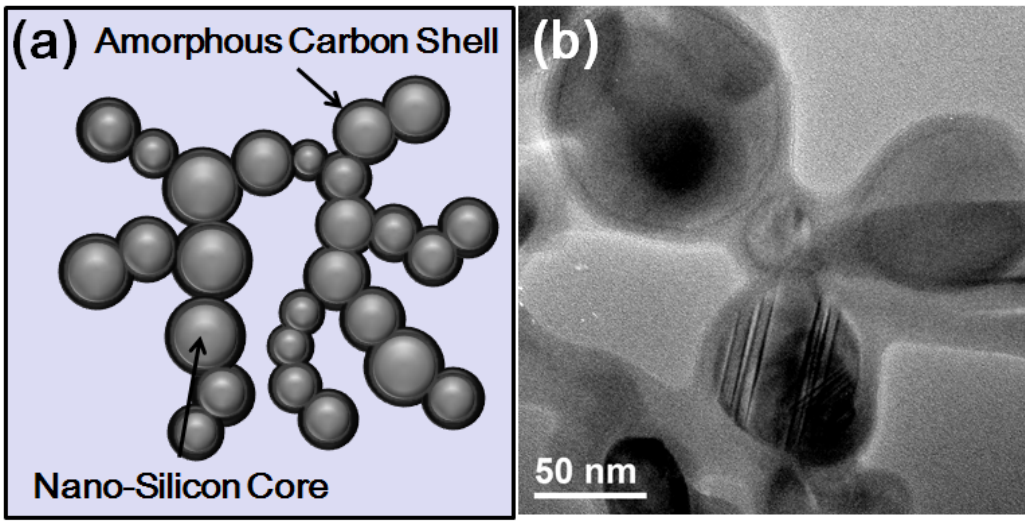

Figure 8. (a) Schematic illustration and (b) bright field TEM image of nano-Si/C core-shell nanostructured material.

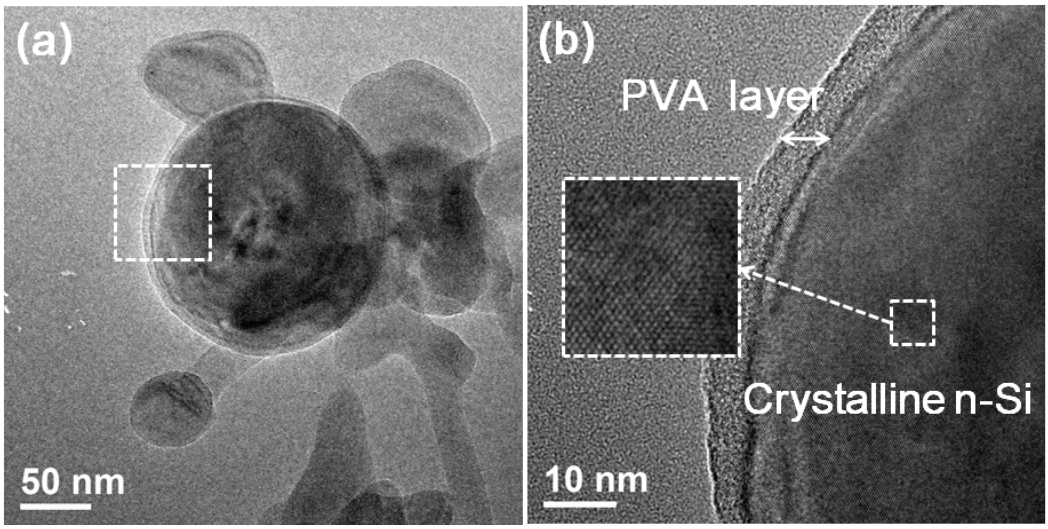

Figure 9. (a) Bright field TEM image and (b) HRTEM image of nano-Si/PVA, respectively.

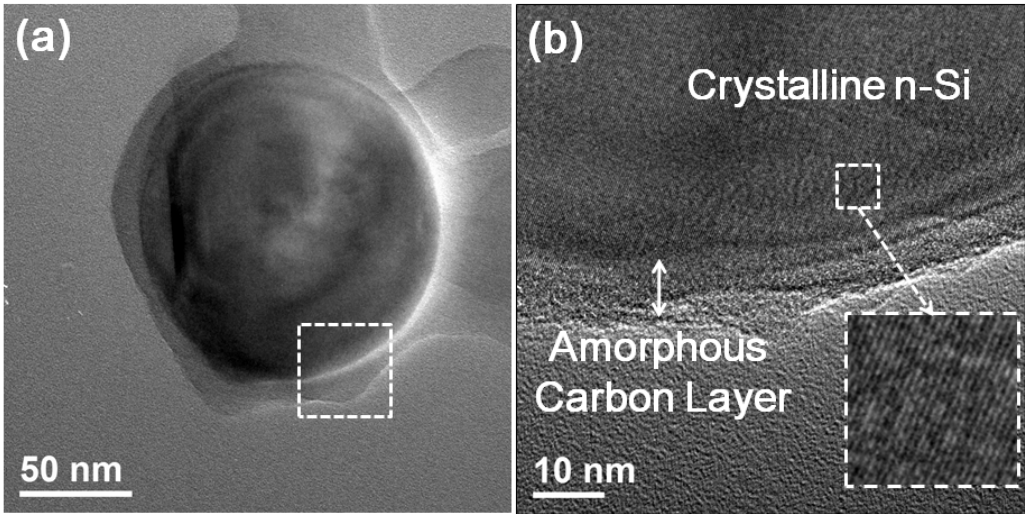

Figure 10. (a) Bright field TEM image and (b) HRTEM image of nano-Si/C core-shell nanostructured material, respectively.

higher than that of nano-Si/PVA from AC impedance measurements. The improvement of electrical conductivity after carbonization of PVA provided easy supply of electron to the whole surface of active Si electrode, and nano-Si/C electrode exhibited much higher capacity than nano-Si/PVA electrode. The shell thickness of carbon was about 5 nm, and the reversible capacity of carbonized PVA (750 ^{o}C) electrode was approximately 100 mAh g^{-1}. Since the carbon content in nano-Si/C core-shell nanostructured electrode was very small, contribution to the total reversible capacity of the nano-Si/C core-shell nanostructured electrode from the carbon layer was negligible. *Ex situ* analyses were conducted to confirm the reaction products during the cycling. Figure 12 shows the *ex situ* XRD patterns of nano-Si/C core-shell nanostructured electrode at the first cycle. When electrode was fully 0 V, $Li_{15}Si_4$ phase appeared, and agreed well with previous studies on the lithiated to reaction mechanism between Li and Si[1,42]. During the discharge step, Si peak in XRD pattern still remained that some of the Si particles did not react with Li completely probably due to the agglomeration of nano-Si/C core-shell nanostructured material during the carbonization process as mentioned previously, which prohibited direct contact between nano-Si/C particles and the electrolyte. This fact could

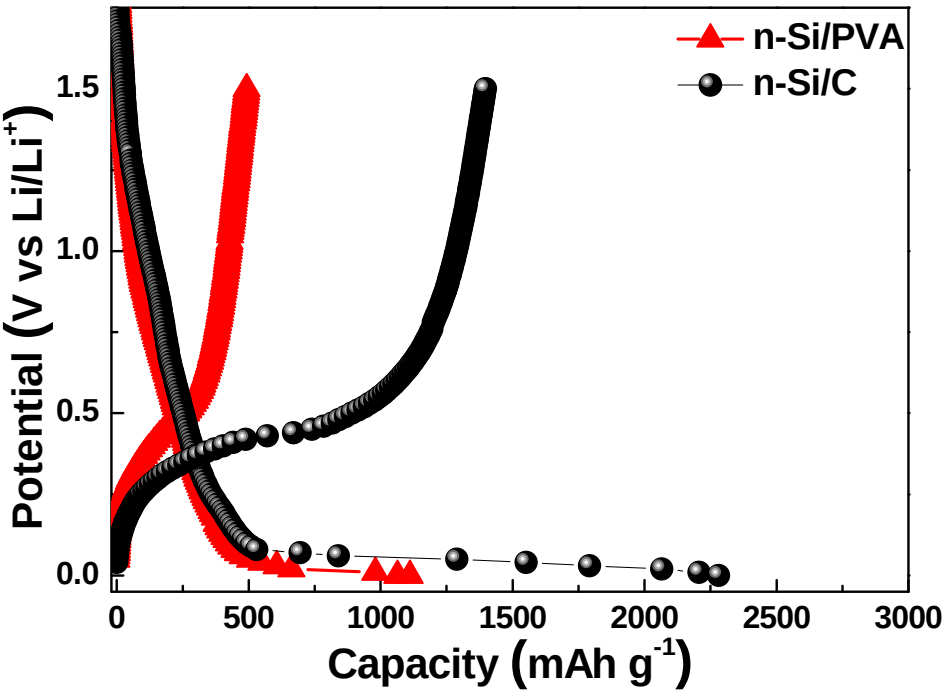

Figure 11. Voltage profiles of nano-Si/PVA and nano-Si/C core-shell nanostructured electrodes.

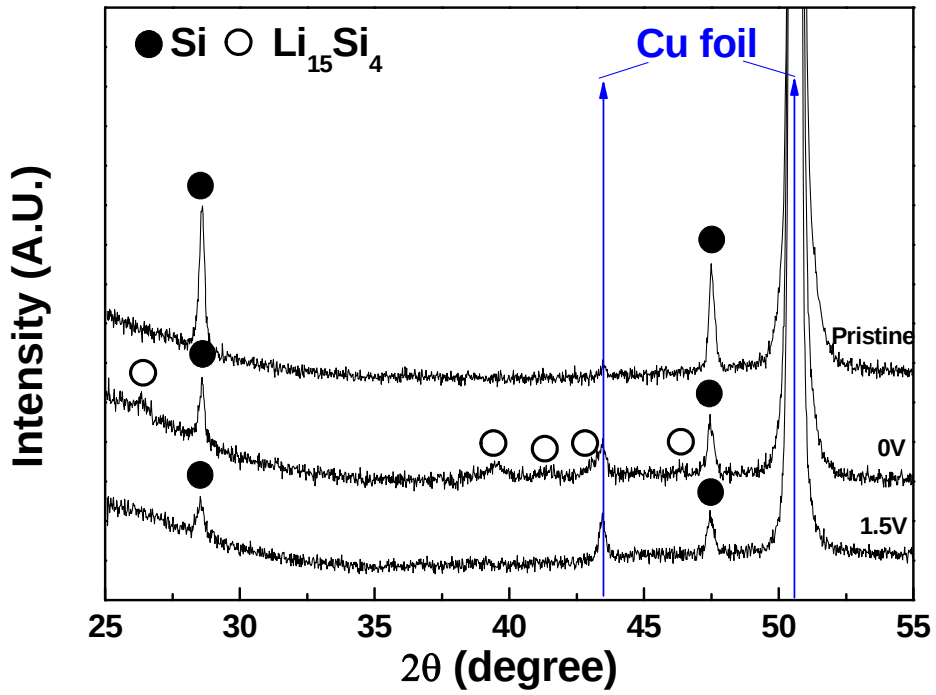

Figure 12. *Ex situ* XRD analysis of the first cycle (pristine, lithiated to 0.0 V, delithiated to 1.5 V).

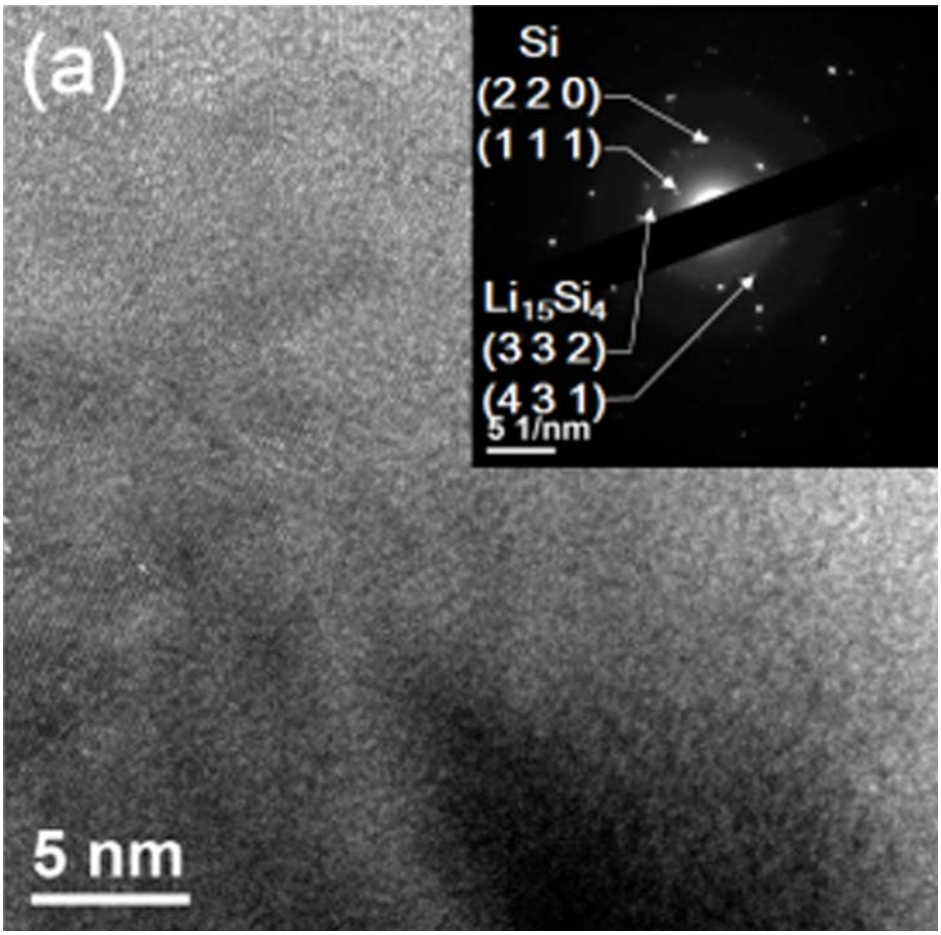

Figure 13. *Ex situ* HRTEM images with SAED of the 1st cycle (a) discharged (lithiated to 0.0 V).

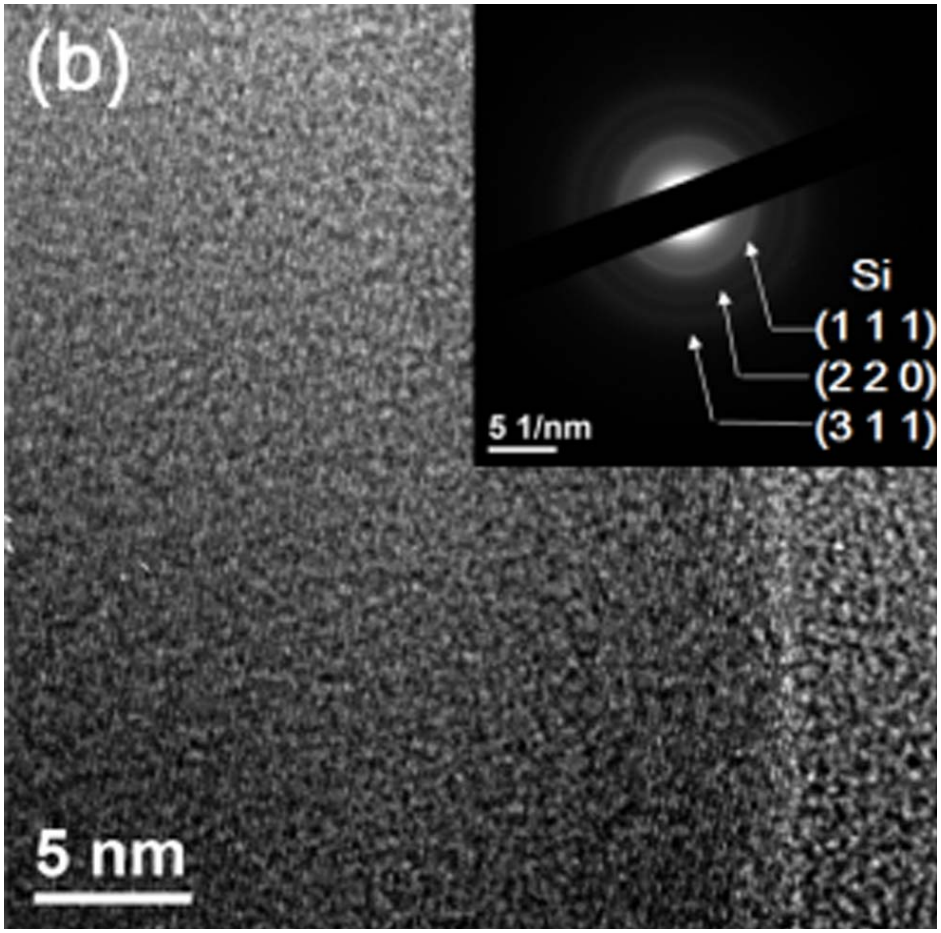

Figure 13. *Ex situ* HRTEM images with SAED of the 1st cycle (b) charged (delithiated to 1.5 V) states.

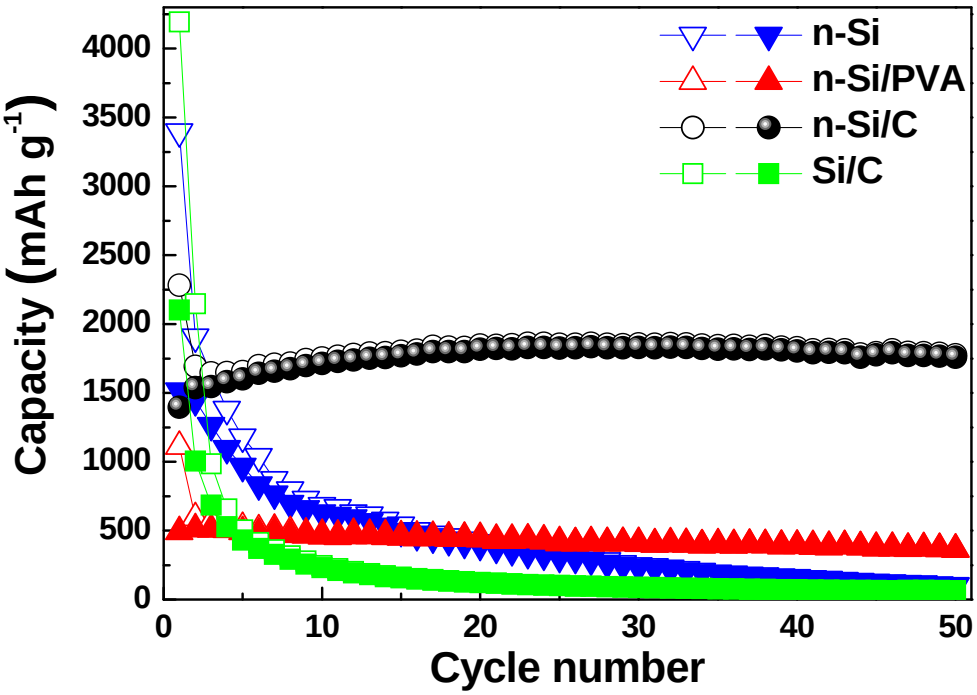

Figure 14. Comparison of cyclability of nano-Si, nano-Si/PVA and nano-Si/C core-shell nanostructured electrodes at the constant current of 100 mA g^{-1}.

explain why the discharge capacity of nano-Si/C core-shell nanostructured electrode at the first cycle was about 2300 mAh g^{-1} which was less than the theoretical capacity of Si at room temperature. When Li was extracted during the charge step, $Li_{15}Si_4$ phase disappeared. From the HRTEM images and selected area electron diffraction (SAED) patterns in figure 13a (fully lithiated at 0 V) and figure 13b. (fully delithiated at 1.5 V), $Li_{15}Si_4$ phase appeared at 0 V and disappeared at 1.5 V while crystalline Si existed at 0 V and 1.5 V, which coincided with the previous XRD data.

Cyclabilities of nano-Si, nano-Si/PVA, nano-Si/C core-shell nanostructured and micron-size Si/C electrodes are compared in figure 14. Micron-sized Si/C electrode prepared by the same method showed a very poor cyclability. It was because micron size Si particle suffered a relatively large volume change during the cycling, and the amorphous carbon shell could not sustain the volume change resulting in dramatic decrease of reversible capacity. On the other hand, nano-Si/PVA electrode also showed a good cycle retention due to the buffering effect of the polymer shell against the volume change during the cycling, but its reversible capacity ($\sim$500 mAh g^{-1}) was small compared with that of nano-Si/C core-shell nanostructured electrode due to a non-conducting nature of coated PVA.

And nano-Si electrode showed about 3500 mAh g^{-1} at the first discharge close to the theoretical capacity at room temperature. However, the capacity decreased dramatically because of volume expansion and contraction during the cycling. Among them, nano-Si/C core-shell nanostructured electrode showed an excellent electrochemical property, and the reversible capacity of 1800 mAh g^{-1}, approximately 5 times larger than graphite electrode, was retained over 50 cycles. Enhanced cyclabilty of nano-Si/C core-shell nanostructured electrode was mainly due to the dual nature of amorphous carbon shell. First, the amorphous carbon shell buffered against volume change of nano-Si crystallites in nano-Si/C core-shell nanostructured electrode during the cycling. Core nano-Si particles were not fractured although expansion/contraction was repeated for many cycles. To confirm the amorphous carbon layer of nano-Si/C core-shell nanostructured electrode which restrained the volume expansion of nano-Si particle during the cycling, TEM image and SAED patterns were obtained after 20 cycles and the results are shown in figure 15. The nano-Si particle was still surrounded by amorphous carbon shell without any indication of crack, and only Si crystallites could be identified from SAED patterns after 20 cycles. Second, enhanced electrical conductivity caused by amorphous carbon

shell[126] after the carbonization of PVA with particle size of core nano-Si under 100 nm[69,125] also contributed the excellent cycle retention. Furthermore, an increase in capacity was observed during the first 15 cycles for nano-Si/C electrode. This phenomenon can be explained by the decreasing of electrochemical impedance due to the insertion of Li ions and expanding the volume of Si particles.[126,127]

Figure 16 shows a rate capability of nano-Si/C electrode indicating superior rate capability. At a rate of 500 mA g^{-1}, reversible capacity was about 1300 mAh g^{-1}, and the reversible capacity at a rate of 1000 mA g^{-1} (approximately 3C rate for the case of graphite electrode) was over 800 mAh g^{-1}. This excellent rate capability was caused by frog spawn shape of core-shell structure in which inner nanosize Si particles under 100 nm was surrounded with electronic conducting amorphous carbon shell. Although the movement of Li^+ through the inside of Si particle was sluggish in general, shorter diffusion path of Li^+ within the nano-size Si in this study was a sig-nificant advantage to get an excellent rate capability.[46,47] This result is comparable to the other nano-Si/C composite anode materials.[128,129] Additionally, the advantage of the process employed in this study was very simple and possible to prepare a large amount of electrode materials at just

one time compare to other processes.

In conclusions, core-shell nanostructured nano-Si/C for Li ion batteries anode material was prepared simply using SIC method followed by carbonizations process. This nano-Si/C core-shell nanostructured material was consists of core Si particles under 100 nm size which were surrounded by electronic conducting amorphous carbon shell of 5 - 10 nm thickness. The unique morphology of nano-Si/C core-shell nanostructured material was similar to frog spawn shape connecting each carbon coated nano-Si particles. The nano-Si/C core-shell nanostructured electrode showed a high capacity (about 1800 mAh g^{-1}) retention, superior rate capability and good cycle retention which were due that the electronic conducting amorphous carbon shell surrounded the nano-size Si particles. This nano-Si/C core-shell nanostructured material which showed excellent electrochemical properties can be produced easily large amounts at one time by SIC method and can be the promising material to replace the carbonaceous anode material for Li-ion batteries.

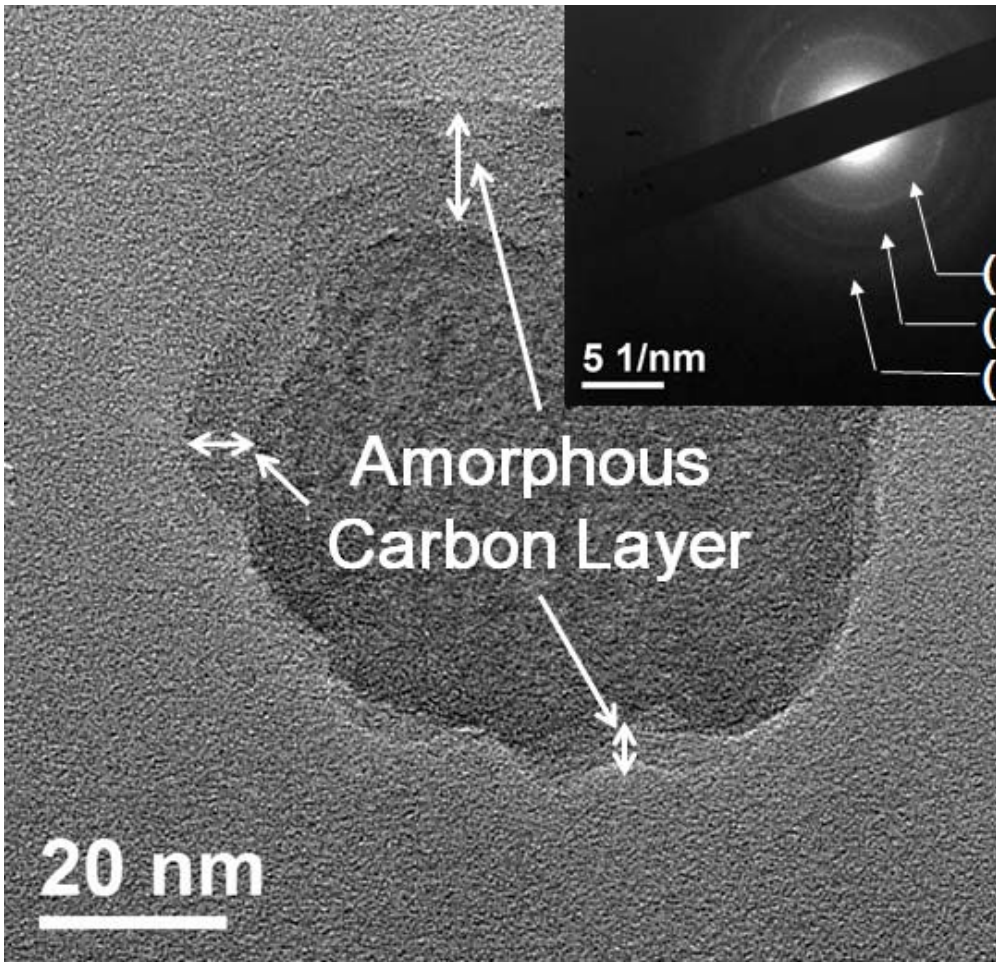

Figure 15. *Ex situ* TEM image with SAED of nano-Si/C core-shell nanastructured electrode of the 20th cycle at fully charge state to 1.5 V.

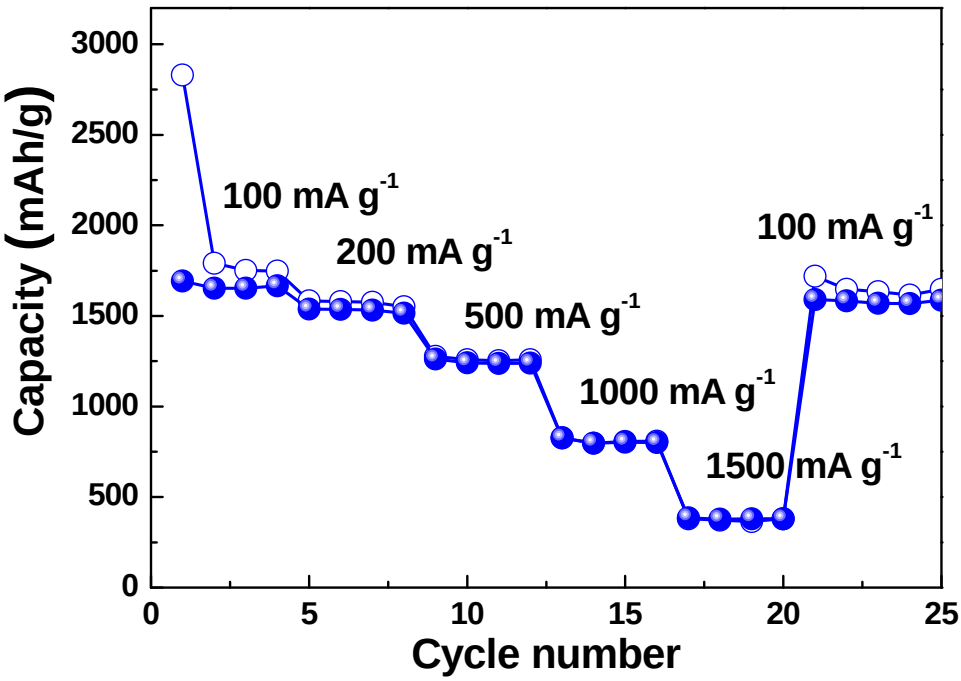

Figure 16. Rate capability test of nano-Si/C core-shell nanostructrued electrode at the various current rates (100 mA g^{-1}, 200 mA g^{-1}, 500 mA g^{-1}, 1000 mA g^{-1}, 1500 mA g^{-1}).

4.2 nano-Si/SnO_2 Core-shell Material

4.2.1 Material Characterization

Figure 17 and figure 18 shows XRD patterns, the EDS concentration profile, and TEM images of the samples. In figure 17, XRD patterns of pristine nano-Si (I) and nano-Si/SnO_2 core-shell nanostructured powders(II) are compared. Broad SnO_2 diffraction peaks(II) appeared, and sharp Si peaks still remained after the coating process. The SnO_2 shells of 5-nm-thickness were almost uniform, as shown in the bright field TEM image (figure 18a). The EDS line scanning profile of the Sn concentration also demonstrated the existence of SnO_2 shells (figure 18b). Figure 18c shows the TEM image of the synthesized SnO_2 hollows pheres.

4.2.2 Electrochemical Characterization

Electrochemical cell tests of the nano-Si, SnO_2 hollow spheres, and nano-Si/SnO_2 core-shell nanostructured electrodes were performed, and the voltage profiles of the first cycle are shown in figure 19. The discharge and charge capacities of the nano-Si/SnO_2 core-shell nanostructured electrode were 2019.8 mAh g^{-1} and 1186.7 mAh g^{-1}, respectively, with a

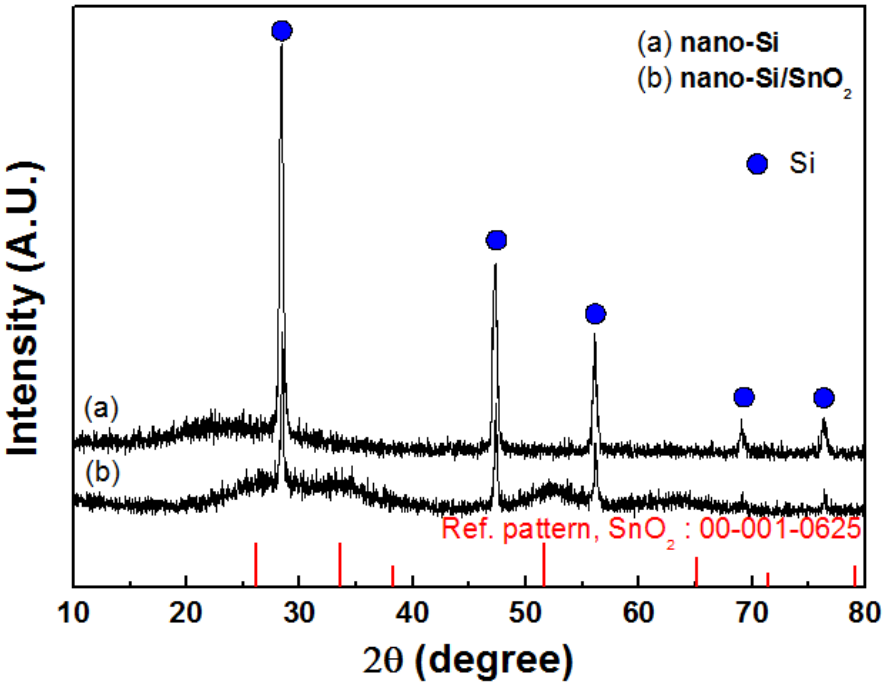

Figure 17. XRD patterns of nano-Si and nano-Si/SnO_2 core-shell nanostructured material.

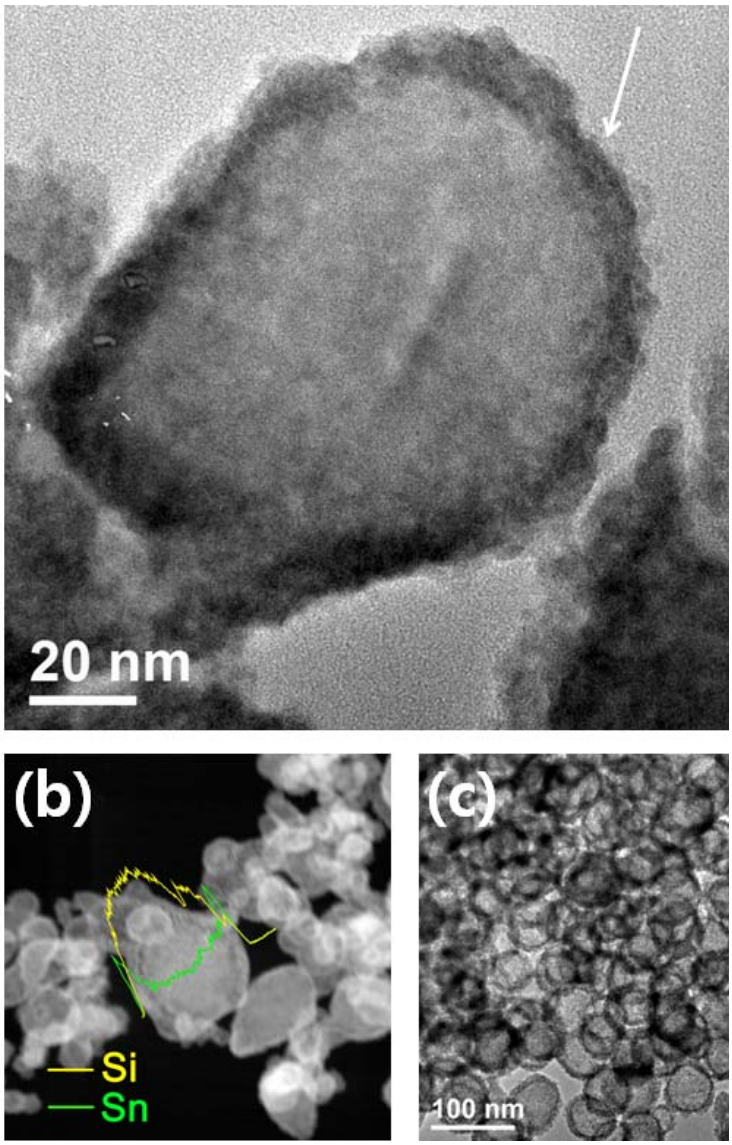

Figure 18. (a) TEM image and (b) EDS concentration profiles for Si and Sn of nano-Si/SnO_2core-shell nanostructured material. (c) TEM image of SnO_2 hollow sphere.

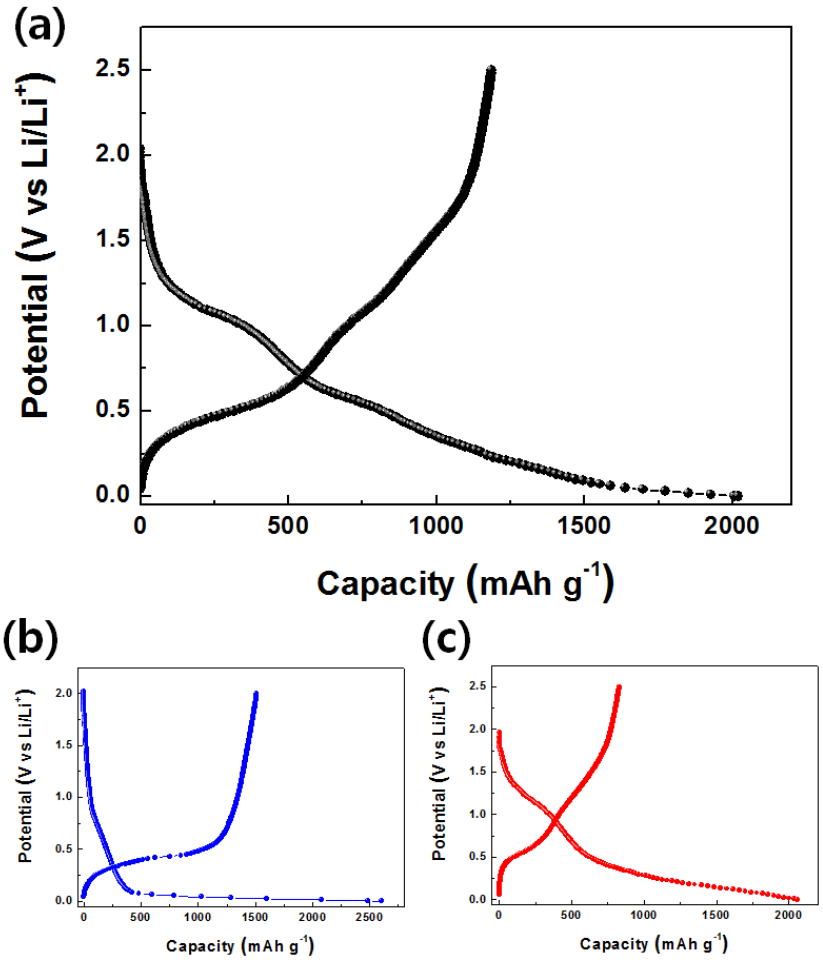

Figure 19. Voltage profiles of (a) nano-Si/SnO_2 core-shell nanostructured, (b) nano-Si and (c) SnO_2 hollow sphere electrodes for the first cycle.

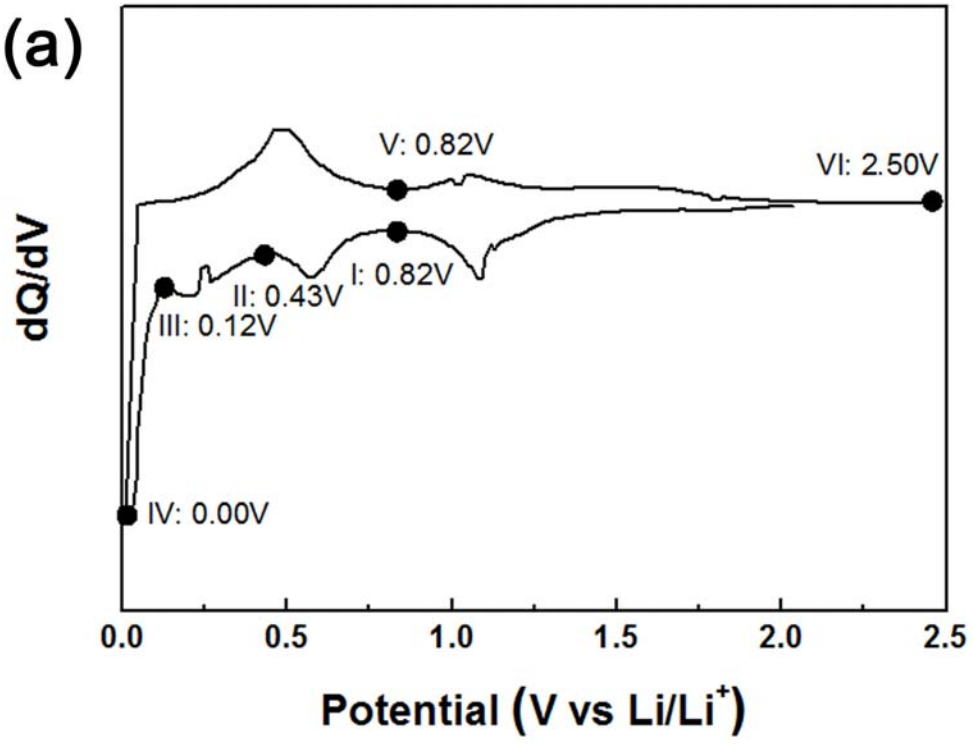

Figure 20. *Ex situ* analyses of nano-Si/SnO_2 core-shell nanostructured electrode. (a) DCP of the nano-Si/SnO_2 core-shell nanostructured electrode for the first cycle.

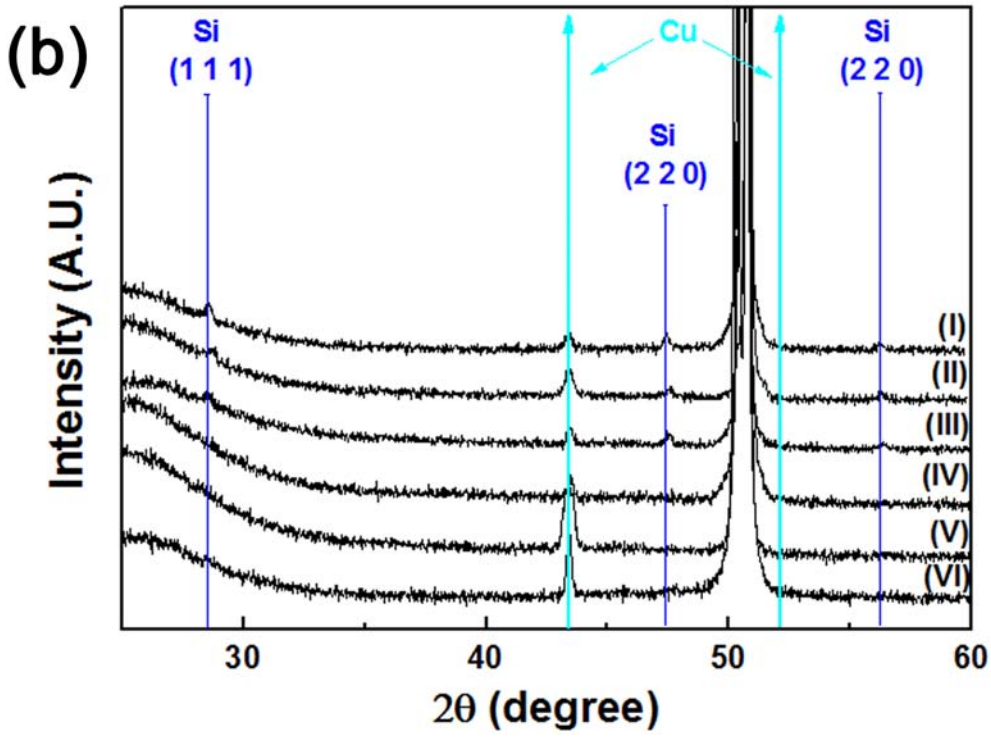

Figure 20. *Ex situ* analyses of nano-Si/SnO_2 core-shell nanostructured electrode. (b) XRD results during the first cycle. Lithiation process: (I) 0.82 V, (II) 0.43 V, (III) 0.12 V, (IV) 0.0 V, Delithiation process: (V) 0.82 V, (VI) 2.50 V.

relatively low Coulombic efficiency of 59 % at the first cycle (figure 19a). At the first discharge, there seemed to be three plateaus near 1.2 V and 0.5 V for SnO_2 (figure 19c), and 0.1 V for the Si electrode (figure 19b).

Figure 20a shows the differential capacity plot (DCP) of the nano-Si/SnO_2 core-shell nanostructured electrode when the electrode was cycled between 2.5 and 0.0 V (vs. Li/Li^+) for the first cycle. *Ex situ* XRD analyses were conducted to establish the reaction mechanism of the nano-Si/SnO_2 core-shell nanostructured electrode at selected potentials, as indicated in DCP. Until the electrode was lithiated to 0.12 V, there were no changes in the diffraction pattern. When the potential reached 0.0 V, the Si peaks disappeared, and no peaks corresponding to Li-Si binary phase or Li-Sn binary phase were observed. During the charging process, only Cu (foil) peaks could be identified.

Figures 21a-e show HRTEM images and selected area electron diffraction (SAED) patterns of the nano-Si/SnO_2 core-shell nanostructured electrode during the first discharge. When the potential was lowered to 0.82 V (figure 21a), unreacted Si and Sn nano-crystallites which were decomposed from SnO_2 were observed (reaction (1.1)), while Li_2O phase

was not identified due to the amorphous nature.[130] At 0.43 V, LiSn was formed (figure 21b) and Li-rich Li_xSn phase appeared at 0.12 V sequentially, while unreacted Si still remained. When the potential reached 0.0 V (figure 21c), only $Li_{22}Sn_5$ phase existed (reaction (1.2)), which agreed with other reports on Sn electrodes.[13,59,130] In general, when the Si electrode was fully lithiated to 0.0 V at room temperature, crystalline $Li_{15}Si_4$ phase was formed.[13] However, no XRD or SAED patterns related to Li-rich Li-Si binary phase were identified at 0.0 V. It is well known that crystalline Si becomes an amorphous Li-Si alloy phase before the formation of crystalline $Li_{15}Si_4$ below 0.05 V during the lithiation process.[13] Therefore, it could be possible that the Li-rich Li-Si binary phase existed at 0.0 V in an amorphous form. To identify the mole fraction of the Li-Si alloy formed at 0.0 V, heat treatment was performed as described in the material characterization section. In figure 21e, crystallized Li-Si alloy phase is shown, which was confirmed as $Li_{12}Si_7$ phase by HRTEM analysis. According to the EDS quantitative analysis results of nano-Si/SnO_2 core-shell nanostructured powder, the weight fractions of Si and SnO_2 were 44.1 wt.% and 55.9 wt.%, respectively.

Based on the EDS results, the first cycle discharge capacity of the SnO_2 hollow spheres and conducting agent was approximately 1200 mAh g^{-1}, and the first discharge capacity from Si was about 800 mA g^{-1} (Li_xSi, x~1.9). With this calculation result and TEM analysis, the mole fraction of Li-Si alloy at 0.0 V was suggested to be close to 1.7 ($Li_{12}Si_7$). According to previous reports, $Li_{12}Si_7$ phase was formed near 0.1 V.[131] This deviation of the potential between the Si electrode and nano-Si/SnO_2 core-shell nanostructured electrode may occur due to the Li_2O/Li-Sn alloy composite layer.

During the charging process (figure 22), metallic Sn that decomposed from $Li_{22}Sn_5$ phase was observed at 0.82 V in figure 22a. Figure 22b shows two different nearby regions when the electrode was fully charged to 2.5 V, in which both Sn and SnO_2 phase were observed. Previous reports suggested that the peak near 1.2 V in DCP during the delithiation process was related to the dealloying process of Li-Sn binary phase.[58] However, the Li-Sn binary phase was already fully decomposed to Sn at 0.82 V, as shown in figure 22a. Thus, the peak near 1.2 V was related to the partial recombination reaction between Sn and Li_2O to form

the SnO_2 phase, which was suggested by Lian et al.[56] and Lou et al.[57] and identified in this study, rather than the dealloying process of Li-Sn binary phase. Therefore, the following reaction mechanisms are suggested :

During lithiation:

$$Si + SnO_2 + 4Li^+ + 4e^-$$

$$\rightarrow Si + Sn + 2Li_2O + (4.4 + x)Li^+ + (4.4 + x)e^-$$

$$\rightarrow Li_{12}Si_7 \text{ (amorphous)} + Li_{4.4}Sn + 2Li_2O \quad (4.1)$$

During delithiation:

$$Li_{12}Si_7 \text{ (amorphous)} + Li_{4.4}Sn + 2Li_2O$$

$$\leftrightarrow Si + (1 - y)Sn + (2 - 2y)Li_2O + ySnO_2 \quad (4.2)$$

After the first cycle, the SnO_2 shells were transformed into $Sn/Li_2O/SnO_2$ composite shell. The sizes of the decomposed Sn crystallites were still 3 ~ 5 nm, and neither grain growth nor agglomeration were observed. Schematic illustration of reaction mechanism is shown in figure 23.

The cyclabilties of nano-Si and n-Si/SnO_2 core-shell nanostructured electrodes are compared and shown in figure 24. The nano-Si electrode showed poor cyclability because of the relatively large volume change

during the cycling, as well as the low electrical conductivity of Si. The nano-Si/SnO_2 core-shell nanostructured electrode showed a reversible capacity of c.a. 1000 mAh g^{-1} and good cycle retention close to 80 % of the first charge capacity over 50 cycles, showing much larger reversible capacity than nano-Si.

The enhanced electrochemical properties of nano-Si/SnO_2 core-shell nanostructured electrode were mainly due to the structural stability of the shells and limited Si reactivity with Li. If the $Li_{15}Si_4$ phase was formed, the electrode would suffer from a large volume change of about 300 %.[132] However, in the case of the nano-Si/SnO_2 core-shell nanostructured electrode, amorphous $Li_{12}Si_7$ phase formed, and the volume change was only 140 %.[132] figure 25a shows the HRTEM bright field image of the electrode material and the nano-Si core.

The shell remained even after 50 cycles. The EDS mapping (figure 25b) demonstrated the presence of Si particles in the core and Sn in the shell region. Based on the reaction chemistry given in reactions (4.1) and (4.2), the shell was composed of Sn/Li_2O/SnO_2. This structural stability contributed the good cyclability of the nano-Si/SnO_2 core-shell

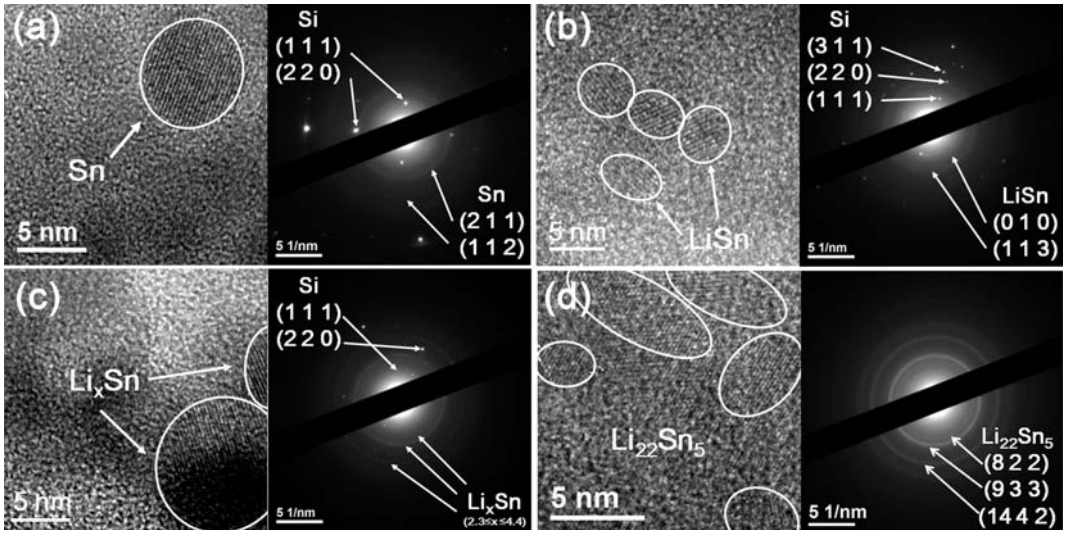

Figure 21. HRTEM images with SAED patterns of the nano-Si/SnO_2 core-shell nanostructured electrode. Lithiation process: (a) 0.82 V, (b) 0.43 V, (c) 0.12 V, and (d) 0.0 V

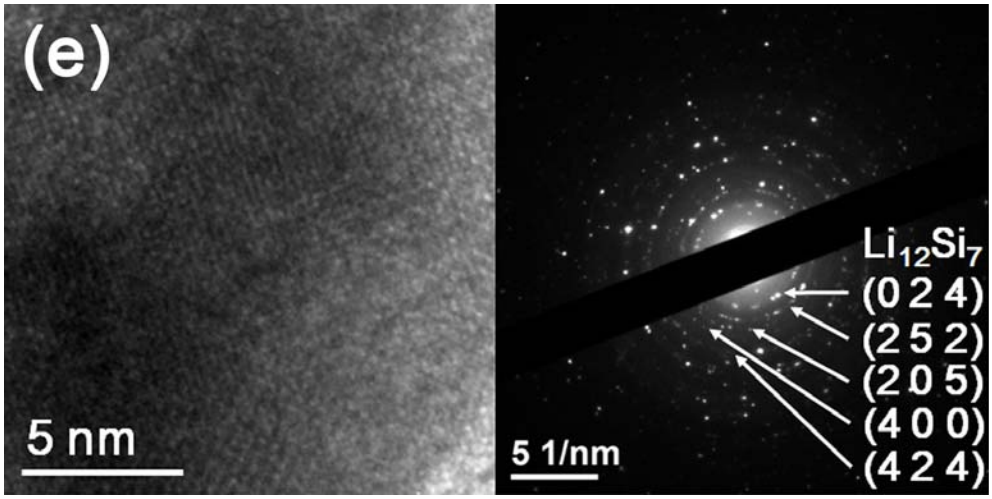

Figure 22. HRTEM images with SAED patterns of the nano-Si/SnO_2 core-shell nanostructured electrode. Lithiation process: (e) 0.0 V, dried and heat-treated at 500 ℃ for 12 h under Ar atmosphere.

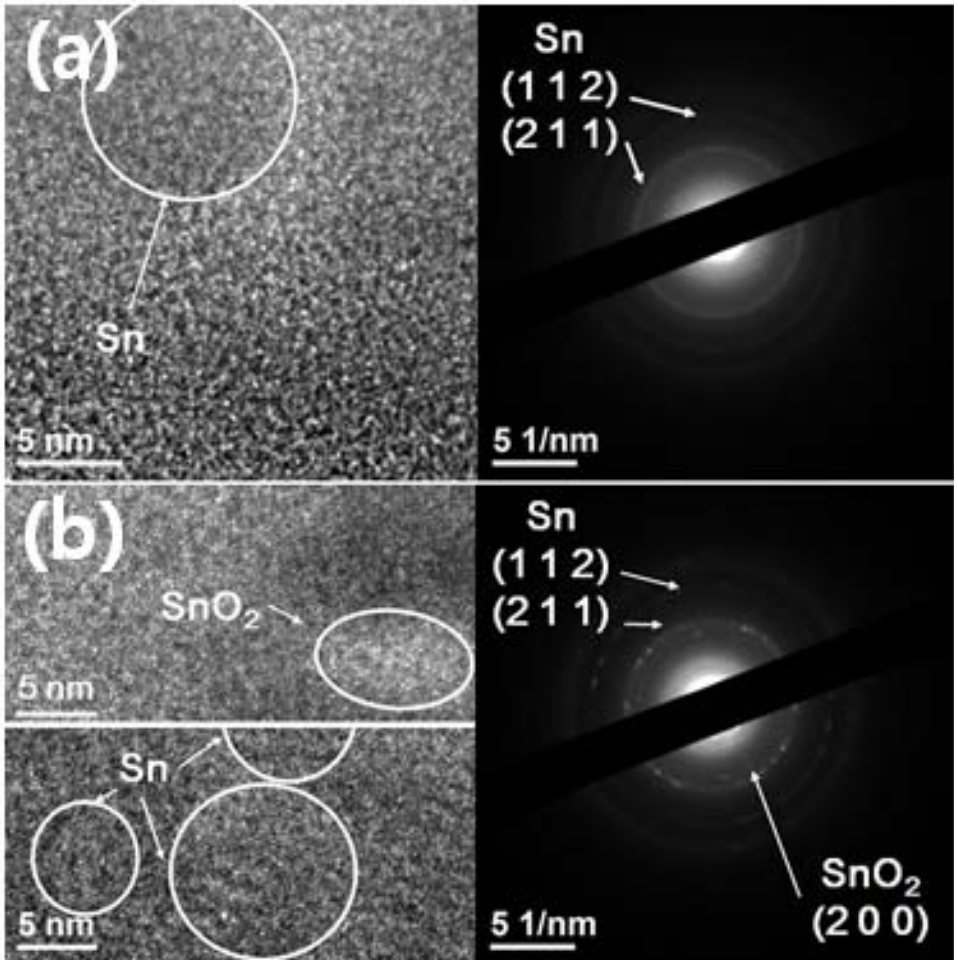

Figure 23. HRTEM images with SAED patterns of the nano-Si/SnO_2 core-shell nanostructured electrode. Delithiation process: (a) 0.82 V, (b) 2.50 V.

Figure 24. Schematic illustration of reaction mechanism of nano-Si/SnO_2 core-shell nanostructured electrode.

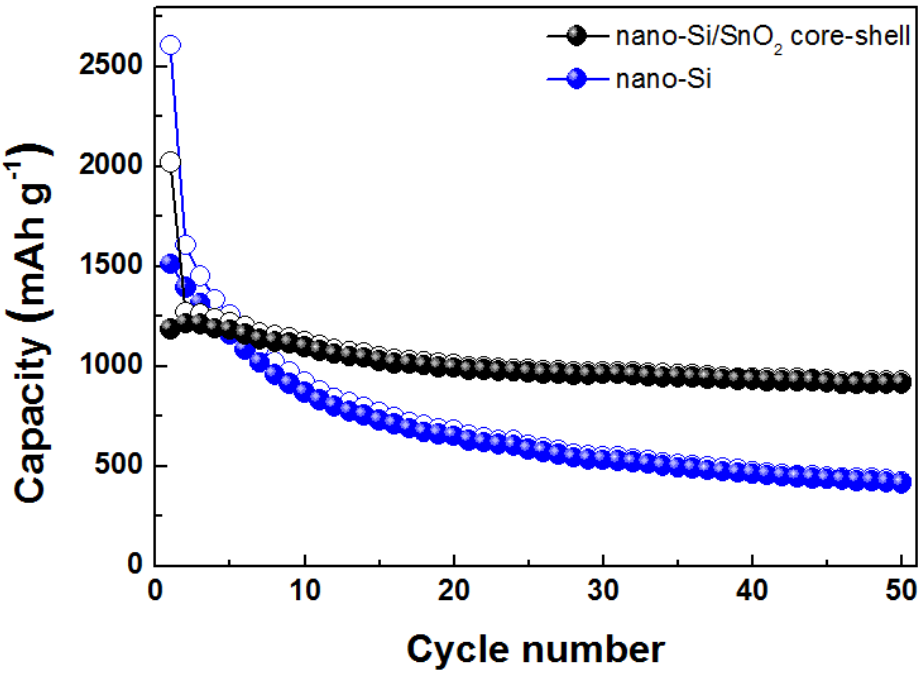

Figure 25. Comparison of cyclabilities for the nano-Si and nano-Si/SnO_2 core-shell nanostructured electrodes.

nanostructured electrode. Compared with a previous report on Si coated onto SnO_2 pore walls,[133] this nano-Si/SnO_2 core-shell nanostructured material could be synthesized in a single step with ease. Figure 26 shows the results of rate capability tests, which indicate excellent rate capability. At a current density of 1.5A g^{-1} (close to 1.5 C rate for the case of nano-Si/SnO_2 core-shell nanostructured electrode and 5 C rate for the case of graphite electrode), the reversible capacity was almost 500 mAh g^{-1}. This excellent rate capability was caused by the inner nano-size Si particles under 100 nm with Sn/Li_2O/SnO_2 shells of ~ 5-nm-thickness. Enhancing the electrical conductivity due to the remaining Sn that had decomposed from SnO_2 after cycling[58] and shorter diffusion path of Li^+ within the nano-Si[46,47] were helpful to improve the rate capability.

In conclusions, An n-Si/SnO_2 core-shell nanostructured electrode was prepared using sol-gel method. The SnO_2 shell of 5-nm-thickness was coated onto Si nanoparticles. Due to this unique shell structure, Sn crystallites did not suffer from agglomeration during charge. The electrode showed a high capacity of about 1000 mAh g^{-1}, and good cycle retention of almost 80 % over 50 cycles, owing to the structural stability of the

shells. These properties were much better than those of the nano-Si electrode. During the lithiation process, SnO_2 was decomposed to Sn and Li_2O, followed by the formation of $Li_{22}Sn_5$ phase. Core Si particles restrictively reacted with Li, forming an amorphous $Li_{12}Si_7$ (amorphous) phase instead of crystalline $Li_{15}Si_4$. When the electrode was delithiated, Si became amorphous, while Sn recombined with Li_2O partially to form SnO_2 phase. This nano-Si/SnO_2 core-shell nanostructured electrode could be a strong candidate as an anode material for LiBs.

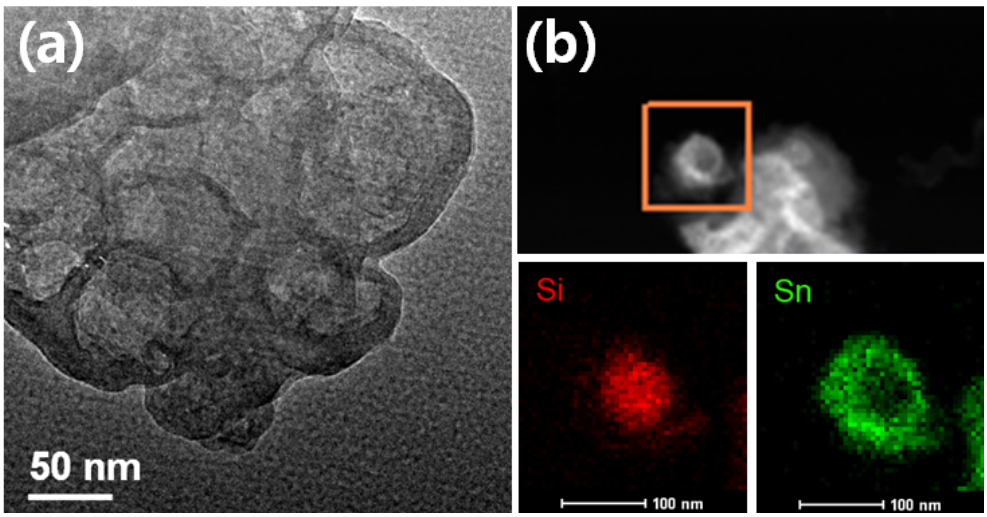

Figure 26. (a) TEM image and (b) EDS mapping images of nano-Si/SnO_2 core-shell nanostructured electrodes of the 50th cycle at 2.5 V.

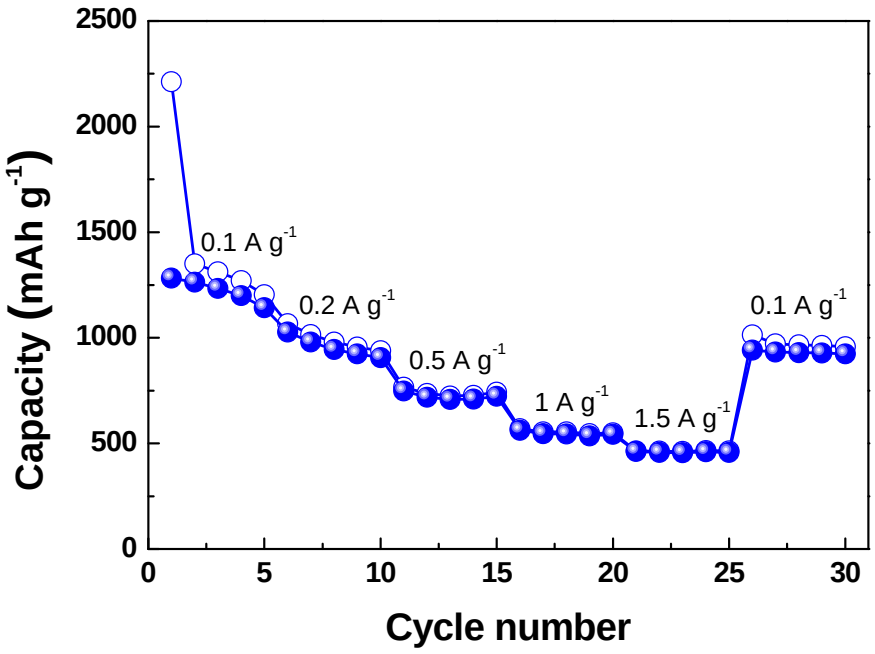

Figure 27. Rate capability test of nano-Si/SnO_2 core-shell nanostructured electrodes at the various current rates (0.1 A g^{-1}, 0.2 A g^{-1}, 0.5A g^{-1}, 1 A g^{-1}, 1.5 A g^{-1}).

Chapter 5. Conclusions

In this thesis, nano-Si/C and nano-Si/SnO_2 core-shell nanostructured material were synthesized by a simple SIC methods and sol-gel method, respectively and tested as anode materials for Li-ion batteries. These core-shell nanostructured electrodes showed much better electrochemical properties than nano-Si electrode. And also reaction mechanism of each electrode was confirmed by various analyses such as *ex situ* XRD and TEM analyses. The following points are summarized.

1. Core - shell nanostructured n-Si/C for Li ion batteries anode material was prepared simply using SIC method followed by carbonizations process. Among various carbon coating techniques, substrate induced coagulation (SIC) method is very efficient tool to prepare a large amount of core-shell structured material at one time. This n-Si/C core-shell nanostructured material was consists of core Si particles under 100 nm size which were surrounded by electronic conducting amorphous carbon shell of 5 - 10 nm thickness. The unique morphology of n-Si/C core-shell material was similar to frog spawn shape connecting each carbon coated n-Si particles.

2. The n-Si/C core-shell nanostructrued electrode showed a high capacity (about 1800 mAh g^{-1}) retention, superior rate capability and good cycle retention which were due that the electronic conducting amorphous carbon shell surrounded the nano-size Si particles.

3. An nano-Si/SnO_2 core-shell nanostructured electrode was prepared using sol-gel method. SnO_2, one of the promising anode material for LiBs by itself, was chosen shell materials to enhance the electrochemical properties of Si electrode. The SnO_2 shell of 5-nm-thickness was coated onto Si nanoparticles.

4. During the lithiation process, SnO_2 was decomposed to Sn and Li_2O, followed by the formation of $Li_{22}Sn_5$ phase. Core Si particles restrictively reacted with Li, forming an amorphous $Li_{12}Si_7$ (amorphous) phase instead of crystalline $Li_{15}Si_4$. When the electrode was delithiated, Si became amorphous, while Sn recombined with Li_2O partially to form SnO_2 phase. Base on the results, higher reversible capacity than the theoretical reversible capacity calculated for eq. (1.1) and (1.2) can be explained. The

electrochemical reaction mechanism of nano-Si/SnO_2 core-shell nanostructured electrode was revealed as follows :

During lithiation:

$$Si + SnO_2 + 4Li^+ + 4e^-$$

$$\rightarrow Si + Sn + 2Li_2O + (4.4 + x)Li^+ + (4.4 + x)e^-$$

$$\rightarrow Li_{12}Si_7 \text{ (amorphous)} + Li_{4.4}Sn + 2Li_2O \qquad (4.1)$$

During delithiation:

$$Li_{12}Si_7 \text{ (amorphous)} + Li_{4.4}Sn + 2Li_2O$$

$$\leftrightarrow Si + (1 - y)Sn + (2 - 2y)Li_2O + ySnO_2$$

5. Due to this unique shell structure, Sn crystallites did not suffer from agglomeration during charge. And the volume change of electrode during cycling is restricted due to the limited reaction of Si. The electrode showed a high capacity of about 1000 mAh g^{-1}, and good cycle retention of almost 80 % over 50 cycles, owing to the structural stability of the shells. These properties were much better than those of the nano-Si electrode.

6. Initial Coulombic efficiency and reversible capacity of nano-Si/C core-shell electrode is higher compare with those of nano-Si/SnO_2 core-shell electrode. However, rate capability of nano-Si/SnO_2 core-shell electrode is better than that of nano-Si/C core-shell electrode.

Excellent electrochemical behaviors and interesting reaction mechanisms of surface modified Si electrode could be a foundation in the development of Si as anode electrode for LiBs. The Electrochemical properties of Si electrode can be changed depending on the shell materials or shell morphology. This researches about surface modified Si electrode can contribute to develop the advanced rechargeable Li-ion batteries.

References

1. G. Jeong, Y.-U. Kim, H. Kim, Y.-J. Kim and H.-J. Sohn, *Energy Environ. Sci* **2011**, 4, 937.
2. G.-A. Nazri and G. Pistoia, *Lithium batteries : Science and Technology* Kluwer academic/Plenum, Boston **2004**.
3. M. Winter, J. O. Besenhard, M. Spahr and P. Novak, *Adv. Mater.* **1998**, 10, 725.
4. M. Winter and R. J. Brodd, *Chem. Rev.* **2004**, 104, 4245
5. J. O. Besenhard, J. Yang and M. Winter. *J. Power Sources* **1997**, 68, 87.
6. J. O. Besenhard, *Handbook of Battery Materials* WILEY-VCH **1999**.
7. T. Agura and K. Tozawa, *Prog. Batt. Solar Cells* **1990**, 9, 209.
8. W. A. Schalkwijk and B. Scrosati, *Advanced in Lithium-Ion Batteries* Kluwer Academic/Plenum, Boston **2002**.
9. R. A. Huggins, *Advanced Batteries : Materials Science Aspects* Springer **2009**.
10. G. Pistoia, *Lithium Batteries : New Materials, Developments and*

Perspectives Elsevier **1994**.

11. D. A. J. Rand, R. Woods and R. M. Dell, *Batteries for Electric Vehicles* SAE INTERNATIONAL **1998**.
12. P. G. Bruce, S. A. Freunberger, L. J. Hardwick and J. M. Tarascon, *Nat. Mater.* **2012**, 11, 19.
13. C.-M. Park, J.-H. Kim, H. Kim and H.-J. Sohn, *Chem. Soc. Rev.* **2010**, 39, 3115.
14. J. R. Dahn, T. Zheng, Y. Liu and J. S. Xue, *Science* **1995**, 270, 590.
15. K. Kang, Y. S. Meng, J. Breger, C. P. Grey and G. Ceder, *Science* **2006**, 311, 977.
16. Y. Oumellal, A. Rougier, G. A. Nazri, J.-M. Tarascon and L. Aymard, *Nat. Mater.* **2008**, 7, 916..
17. X. Y. Song and K. Kinoshita, *J. electrochem. Soc.* **1996**, 145, L120.
18. C. J. Wen, and R. A. Huggins, *J. Power Sources* **1981**, 37, 271.
19. C. K. Chan, H. Peng, G. Liu, K. Mcilwrath, X. F. Zhang, R. A. Huggins and Y. Cui, *Nat. Nanotech.* **2008**, 3, 31.
20. H. Jung, Y.-U. Kim, M.-S. Sung, Y. Hwa, G. Jeong, G. B. Kim and H.-J. Sohn, *J. Mater. Chem.* **2011**, 21, 11213.

21. A. Magasinski, P. Dixon, B. Hertzberg, A. Kvit, J. Ayala and G. Yushin. *Nat. Mater*. **2010**, 9, 353.

22. L. Baggetto and P. H. Notten, *J. Electrochem. Soc.* **2009**, 156, A169.

23. Y. Hwa, C. M. Park, S. Yoon and H.-J. Sohn, *Electrochim. Acta* **2010**, 55, 3324.

24. J. Graetz, C. C. Ahn, R. Yazami and B. Fultz, *J. Electrochem. Soc.* **2004**, 151, A698.

25. C. J. Wen and R. A. Huggins *J. Solid-State Chem.* **1980**, 35, 376.

26. J. Hassoun, G. Derrien, S. Panero and B. Scrosati, *Adv. Mater*. **2008**, 20, 3169.

27. M. Winter and J. O. Besenhard, *Electrochim. Acta* **1999**, 45, 31.

28. W.-S. Kim, Y. Hwa, J.-H. Jeun, H.-J. Sohn, and S.-H. Hong, *J. Power Sources* **DOI:10.1016/j.jpowsour.2012.10.030**.

29. Y. Hwa, W.-S. Kim, S.-H. Hong and H.-J. Sohn, *Electrochimica Acta* **2012**, 71, 201.

30. Y. Hwa, C.-M. Park and H.-J. Sohn, *J. Power Sources* **2013**, 222, 129.

31. C.-M. Park and H.-J. Sohn, *Adv. Mater.* **2007**, 19, 2465.

32. C.-M. Park, Y.-U. Kim and H.-J. Sohn, *Chem. Mater.* **2009**, 21, 5566.

33. Y.-U. Kim, B. W. Cho and H.-J. Sohn, *J. Electrochem. Soc.* **2005**, 152, A1475.

34. C.-M. Park, S. Yoon, S.-I. Lee, J.-H. Kim, J.-H. Jung and H.-J. Sohn, *J. Electrochem. Soc.* **2007**, 154, A917.

35. C.-M. Park and H.-J. Sohn, *Adv. Mater.* **2010**, 22, 47.

36. L. M. L. Fransson, J. T. Vaughey, K. Edstrom and M. M. Thackeray, *J. Electrochem. Soc.* **2003**, 150, A86.

37. W. Xianming, T. Nishina and I. Uchida, *J. Power Sources* **2002**, 104, 90.

38. C.-M. Park, H. Jung and H.-J. Sohn, *Electrochem. Solid-State Lett.* **2009**, 12, A171.

39. H. Wu, G. Chan, J.-W. Choi, I. Ryu, Y. Yan, M. T. McDowell, S.-W. lee, A. Jackson, Y. Yang, L. Hu and Y. Cui, *Nat. Nanotech.* **2012**, 7, 310.

40. M. S. Whittingham and A. J. Jacobson, *Intercalation Chemistry* Academic Press, New York, **1982**.

41. M. S. Dresselhaus, *Intercalatioin Layerd Materials* Plenum Press New York, **1986**.

42. M. N. Obrovac and L. Chrstensen, Electrochem. Solid-State Lett. 2004, 7, A93

43. J. Li and J. R. Dahn, *J. Electrochem. Soc.* **2007**, 154, A156.

44. H. Zhang, L. Yang, I. Fu, Q. Cao, D. Sun, Y. Wu and R. K. Holze, *Solid State Chem.* **2009**, 13, 1521.

45. T. Kim, S. Park and S.-M. Oh, *Electrochem. Commun.* **2006**, 8, 1461.

46. L. F. Cui, R. Ruffo, C. K. Chan, H. L. Peng and Y. Cui, *Nano Lett.* **2009**, 9, 491.

47. J. Maier, *J. Power Sources* **2007**, 174, 569.

48. S. Iwamura, H. Nishihara and T. Kyotani, *J. Phy. Chem. C* **2012**, 116, 6004.

49. M. T. McDowell, S.-W. Lee, I. Ryu, H. Wu, W. D. Nix, J.-W. Choi and Y. Cui, *Nano Lett.* **2011**, 11, 4018.

50. Y. Yu, L. Gu, C. Zhu, S. Tsukimoto, P. A. V. Aken and J. Maier, *Adv. Mater.* **2010**, 22, 2247.

51. Y. S. Hu, R. Demir-Cakan, M. M. Titirici, J. O. Muller, R. Schlogl, M. Antonietti and J. Maier, *Angew. Chem. Int. Ed.* **2008**, 47, 1645.

52. N. Dimov, S. Kugino and M. Yoshio, *Electrochim. Acta* **2003**, 48,

1579.

53. A. Basch, B. Gollas, R. Horn and J. O. Besenhard. *J. Appl. Electrochem.* **2005**, 35, 169.
54. K. W. Leitner, J. O. Besenhard and M. Winter, *J. Power Sources* **2005**, 146, 209.
55. C. Kim, M. Noh, M. Choi, J. Cho and B. Park, *Chem. Mater.* **2005**, 17, 3297.
56. P. Lian, X. Zhu, S. Liang, Z. Li, W. Yang and H. Wang, *Electrochim. Acta* **2011**, 56, 4532.
57. X. W. Lou, J. S. Chen, P. Chen and L. A. Archer, *Chem. Mater.* **2009**, 21, 2868.
58. G. Du, C. Zhong, P. Zhang, Z. Guo, Z. Chem and H. Liu, *Electrochim. Acta* **2010**, 55, 2582.
59. I. A. Courtney and J. R. Dahn, *J. Electrochem. Soc.* **1997**, 144, 2045.
60. M. S. Whittingham, *Science* **1976**, 192, 1126.
61. C.-M. Park, *Ph.D. dissertation*, Seoul National University, **2009**.
62. S. Megahed and B. Scrosati, *J. Power Sources* **1994**, 51, 79.
63. R. Alberty, R. Silbey, *Physical Chemistry*; John Wiley : New York,

1996.

64. S. Flandrois, B. Simon, *Carbon* **1999**, 37, 165.
65. J.-H. Kim, H. Kim, H.-J. Sohn, *Electorchem. Comm.* **2005**, 7, 557.
66. S. Yoon, I.-S. Lee, H. Kim, H.-J. Sohn, *J. Power Sources* **2006**, 161, 1319.
67. Y. Hwa, C.-M. Park, S. Yoon, H.-J. Sohn, *Electrochim. Acta* **2010**, 55, 3324.
68. J. Yang, M. Wachtler, M. Winter, J. O. Besenhard, Electrochem. *Solid State Lett.* **1999**, 2, 161.
69. J. Yang, M. Winter, J. O. Besenhard, *Solid State Ionics* **1996**, 90, 281.
70. M. Wachtler, M. Winter, J. O. Besenhard, *J. Power Sources* **2002**, 105, 151.
71. J. O. Besengard, J. Yang, M. Winter, *J. Power Sources* **1997**, 68, 87.
72. K. C. Hewitt, L. Y. Beaulieu, J. R. Dahn, *J. Electrochem. Soc.* **2001**, 148, A402.
73. J. T. Vaugheya, L. Franssonb, H. A. Swingera, K. Edstrom, M. M. Thackeray, *J. Power Sources* **2003**, 119, 64.
74. H. Honda, H. Sakahuchi, I. Tanaka, T. Esaka, *J. Power Sources* **2003**,

123, 216.

75. H. Honda, H. Sakahuchi, Y. Fukuda, T. Esaka, *Mater. Res. Bull.* **2003**, 38, 647.

76. K. Xu, *Chem. Rev.* **2004**, 104, 4303

77. R. Nave, *Abundances of the elements in the Earth's Crust*, Georgia State University.

78. W. C. O'Mara, *Handbook of Semiconductor Silicon Technology* William Andrew Inc. **2008**, ISBN 0-8155-1237-6, 349-352.

79. H. Kim, J. Choi, H.-J. Sohn and T. Kang, *J. Electrochem. Soc,* **1999**, 146, 4401.

80. H.-Y. Lee and S.-M. Lee, *J. Power Sources*, **2002**,112, 649.

81. W.-G. Lee and J.-G. Lee, *J. Electrochem. Soc*, **2002**, 149, G1.

82. J. Wolfenstine, *J. Power Sources,* **2003**, 124, 241.

83. M. K. Datta and P. N. Kumta, *J. Power Sources,* **2006**, 158, 557.

84. W. Wang, M. N. Datta and P. N. Kumta, *J. Mater. Chem,* **2007**, 17, 3229.

85. Y. Liu, K. Hanai, T. Matsumura, N, Imanishi, A. Hirano and Y, Takeda, *Electrochem. Solid State Lett.* **2004**, 7, A492.

86. T. Morita and N. Takami, *J. Electrochem. Soc,* **2006**, 153, A425.

87. Y. Zheng, J. Yang, J. Wang and Y. NuLi, *Electrochim. Acta* **2007**, 52, 5863.

88. J. Wang, H. Zhao, J. He, C. Wang and J. Wang, *J. Power Sources* **2001**, 196, 4811.

89. J.-H. Kim, H.-J. Sohn, H. Kim, G. Jeong and W. Choi, *J. Power Sources* **2007**, 170, 456.

90. C.-M. Park, W. Choi, Y. Hwa, J.-H. Kim, G. Jeong and H.-J. Sohn, *J. Mater. Chem.* **2010**, 20, 4854.

91. M. Miyachi, H. Yamamoto, H. Kawai, T. Ohta and M. J. Shirakata, *J. Electrochem. Soc.* **2005**, 152, A2089.

92. J. Yang, Y. Takeda, N. Imanishi, C. Capiglia, J.Y. Xie and O. Yamamoto, *Solid State Ionics* **2002**, 152-153, 125.

93. M. Miyachi, H. Yamamoto and H. Kawai, *J. Electrochem. Soc.* **2007**, 154, A376.

94. T. Kim, S. Park and S.M. Oh, *J. Electrochem. Soc.* **2007**, 154, A1112.

95. Y. Nagao, H. Sakaguchi, H. Honda, T. Fukunaga and T. Esaka, *J. Electrochem. Soc.* **2004**, 151, A1572.

96. J.-H. Kim, C.-M. Park, H. Kim, Y.-J. Kim and H.-J. Sohn, *J. Electroanal. Chem.* **2011**, 1, 664.

97. W.-S. Chang, C.-M. Park, J.-H. Kim, Y.-U. Kim, G. Jeong and H.-J. Sohn, *Energy Environ. Sci.* **2012**, 5, 6895.

98. B. Hertzberg, A. Alexeev and G. Yushin, *J. Am. Chem. Soc,* **2010**, 132, 8548.

99. J. K. Lee, K. B. Smith, C. M. Hayner and H. H. Kung, *Chem. Comm.* **2010**, 46, 2025.

100. T. Song, J. Xia, J.-H. Lee, D.-H. Lee, M.-S. Kwon, J.-M. Choi, J. 쪄, S.-K. Doo, H. Chang, W.-I. Park, D.-S. Zang, H. Kim, Y. Huang, K.-C. Hwang, J. A. Rogers and U. Paik, *Nano Lett.* **2010**, 10, 1710.

101. L. Su, Y. Jing and Z. Zhou, *Nanoscale* **2011**, 3, 3967.

102. Y.-S. Jung, K.-T. Lee and S.-M. Oh, *Electrochim Acta* **2007**, 52, 7061.

103. L.-F. Cui, Y. Yang, C.-M. Hsu and Y. Cui, *Nano Lett.* **2009**, 9, 3370.

104. Y. Xu, G. Yin, Y. Ma, P. Zuo and X. Cheng, *J. Mater. Chem*, **2010**, 20, 3216.

105. H.-X. Ji, X.-L. Wu, L.-Z. Fan, C. Krien, I. Fieringm Y.-G. Guo, Y. Mei and O. G. Schmidt, *Adv. Mater.* **2010**, 22, 4591.

106. P. Balaya, H. Li, L. Kienle and J. Maier, *Adv. Funct. Mater.* **2003**, 13, 621.

107. D. Arumugam and G. P. Kalaignan, *Electrochim. Acta,* **2010**, 55, 8709.

108. F. Wu, M. Wang, Y. F. Su, L. Y. Bao and S. Chen, *Electrochim. Acta* **2009**, 54, 6803.

109. D. Chen, L. Tang and J. Li, *Chem. Soc. Rev.* **2010**, 39, 3157.

110. S. L. Chou, J. Z. Wang, M. Choucair, H. K. Liu, J. A. Stride and S. X. Dou, *Electrochem. Commun.* **2010**, 12, 303.

111. G. Wang, B. Wang, X. Wang, J. Park, S. Dou, H. Ahn and K. Kim, *J. Mater. Chem.* **2009**, 19, 8378.

112. P. Lian, X. Zhu, H. Xiang, Z. Li, W. Yang and H. Wang, *Electrochim. Acta* **2010**, 56, 834.

113. Y. Li, X. Lv, J. Lu and J. Li, *J. Phys. Chem. C* **2010**, 114, 21770.

114. D. W. Choi, D. H. Wang, V. V. Viswanathan, I. T. Bae, W. Wang, Z. M. Nie, J. G. Zhang, G. L. Graff, J. Liu, Z. G. Yang and T.

Duong, *Electrochem. Commun.* **2010**, 12, 378.

115. Z. Chen and J. R. Dahn, *Electrochem. Solid-State Lett.* **2003**, 6, A221.

116. S. K. Hu, G. H. Cheng, M. Y. Cheng, B. J. Hwang and R. Santhanam, *J. Power Sources* **2009**, 188, 564.

117. D. Q. Liu, X. Q. Liu and Z. Z. He, *J. Alloys Compd.* **2007**, 436, 387.

118. A. Basch and J. H. Albering, *J. Power Sources,* **2011**, 196, 3290.

119. A. Basch, B. Gollas, R. Horn and J. O. Besenhard, *J. Appl. Electrochem.* **2005**, 35, 169.

120. K. W. Leitner, J. O. Besenhard and M. Winter, *J. Power Sources* **2005**, 146, 209.

121. P. Scherrer. *Nachr. Ges. Wiss. Gottingen,* **1918**, 26, 98.

122. Wikipedia, http://en.wikipedia.org/wiki/File:Bragg_diffraction_2.svg.

123. Wikipedia, http://en.wikipedia.org/wiki/File:Schema_MEB_(en).svg.

124. Wikipedia, http://en.wikipedia.org/wiki/File:Scheme_TEM_en.svg.

125. H. Li, Q. Wang, L. Shi, I. Chen and X. Huang, *Chem. Mater.* **2002**, 14, 103

126. J. Wang, X. Zhang, J. Liu, G. Yang, Y. Ge and Z. Yu, *Electrochim. Acta* **2010,** 55, 6879.

127. H. Li, X. Huang, L. Chen, G. Zhou, Z. Zhang, D. Yu, Y.J. Mo and N. Pei, *Solid State Ionics* **2000**, 135, 181.

128. J. Guo, A. Sun, X. Chen, C. Wang and A. Manivannan, *Electrochim. Acta* **2011**, 56, 3981.

129. Q. Si, K. Hanai, N. Imanishi, M. Kubo, A. Hirano, Y. Takeda and O. Yamamoto, *J. Power Sources* **2009**, 189, 761.

130. C.-M. Wang, W. Xu, J.-G. Zhang, L. V. Saraf, B. W. Arey, D. Choi, Z.-G. Yang, S. Thevuthasan and D. R. Baer, *Nano Lett.* **2011**, 11, 1874.

131. P. Limthongkul, Y.-I. Jang, N. J. Dudney and Y.-M. Chiang, *Acta Materialia* **2003**, 51, 1103.

132. M. N. Obrovac, L. Christensen, D. B. Le and J. R. Dahn, *J. Electrochem. Soc.* **2007**, 154, A849.

133. W.-J. Lee, M.-H. Park, Y. Wang, J. Y. Lee and J. Cho, *Chem. Comm.* **2010**, 46, 622.

초 록

요즘, 에너지 저장 시스템은 에너지 문제를 해결하는 데 있어서 중요한 화두거리이다. 현재 제시된 에너지 저장 시스템으로는 납축전지, 니켈-카드뮴 전지, 리튬-황 전지, 그리고 리튬 이온 전지 등이 있다. 그 중에서 리튬-이온 전지는 큰 에너지 밀도를 가지고 있어 가장 가능성이 큰 에너지 저장 시스템 중 하나로 꼽히고 있다. 현재 상용화되어 있는 리튬-이온 전지에는 탄소계 음극이 적용되어 있다. 하지만 탄소계 음극은 작은 용량과 고속 충방전 특성에 적합하지 않아 진보된 전자기기에 적용하기에는 적합하지 않다. 이러한 이유로, 향상된 특성을 가지는 리튬-이온 전지용 음극을 개발하기 위한 연구는 계속 진행되어야 한다.

탄소계 음극의 단점을 개선하기 위해서, 많은 연구자들이 탄소계 전극 물질을 대체할 물질을 찾으려 노력하고 있다. 그 중에서도, 실리콘 기반 전극 물질은 큰 용량과 낮은 작동 전압을 가지고 있어서 탄소계 전극 물질을 대체할 후보로써 매우 각광받고 있다. 하지만, 실리콘 기반 전극은 기본적으로 충방전이 진행되는 동안 커다란 부피 변화을 겪게 되어 그 특성에 영향을 주게 되고, 고속 충방전 특성 또한 좋지 않다. 특히 충방전 중 겪게 되는 커다란 부피 변화는 실리콘의 파괴를 일으키게 되고 그로 인해 파괴된 입자는 전기적인 접촉을 잃어버리

게 된다. 그리고 또한 계속된 부피 변화로 인해 SEI 층이 반복적으로 형성되게 되며 이 또한 전기화학적 특성에 않좋은 영향을 미치게 된다.

본 연구에서는 실리콘 전극의 전기화학적 특성을 향상시키기 위해 전도성을 가진 탄소와 주석 산화물을 각각 실리콘 입자 위에 코팅하였다. 전도성을 가진 탄소는 전극의 전기화학적 특성을 향상시키기 위해 자주 쓰이는 코팅 물질 중 하나이고 주석 산화물은 그 훌륭한 전기화학적 특성으로 인해 스스로가 음극 활물질로써의 가치를 가지고 있는 물질이다. 이 물질들을 각각 실리콘과 조합함으로써 실리콘 전극은 음극 물질로써의 그 특성이 매우 향상 될 수 있다. 이러한 가능성을 기반으로 만들어진 표면 개질된 실리콘 전극의 전기화학적 특성을 시험하였고, 그 결과 각각의 전극이 모두 훌륭한 특성을 나타냄을 확인하였다. 그리고 또한 각 전극의 리튬과의 반응 기구를 규명하였다. 결과적으로 본 연구를 통해 표면 개질된 코어-셸 나노 구조를 가진 실리콘 전극은 탄소계 전극을 대체할 강력한 후보로써의 가치가 있음을 확인하였다.

주요어 : 리튬-이온 전지, 음극 물질, 실리콘, 코어-셸 구조, 전기화학, 주석 산화물, 탄소.

학번 : 2007-20752

감사의 글

‘나 스스로에게 당당하기 위해, 노력을 게을리 하지 말자’ 이 말을 가슴에 품고 연구를 시작한지 6년 째, 여전히 미흡하지만 나름의 노력 끝에 박사학위를 받게 되었습니다. 비록 박사학위라는 호칭 앞에서 느껴지는 스스로의 부족함과 무게감에 지레 걱정이 되기도 하지만, 지금 이 순간이 끝이 아닌 시작임을 잊지 말고 부족함과 아쉬움을 양분삼아 더 나아가려 합니다.

우선, 6년이라는 시간동안 사람으로서, 그리고 연구자로서의 수많은 가르침을 주신 손헌준 선생님께 머리 숙여 감사한 마음을 전해드리고 싶습니다. 2006년 11월 어느 날, 배터리 연구를 하고 싶다며 무턱대고 찾아간 저를 “무엇보다도 사람으로서의 본분을 잊지 말라”는 말씀과 함께 연구실의 일원으로 받아주셨던 선생님의 모습을 저는 여전히 생생하게 기억하고 있습니다. 대학원 생활 동안, 선생님께서 주신 주옥같은 가르침들을 하나하나 가슴 깊이 새겨 앞으로의 삶의 지표로 삼고 올바른 삶을 살도록 노력하겠습니다.

그리고 부족한 제 논문을 지도해 주신 이정중 교수님과 박병우 교수님께도 진심으로 감사의 말씀 드립니다. 굳은 날씨에도 먼 길 마다않고 후배의 논문을 지도해 주신 김한수 교수님과 김재헌 박사님께도 함께 감사드립니다.

지난 6년동안 내 시간의 대부분을 보냈던 ‘전지 및 전해공정 실험실’ 선배님들 그리고 하나 뿐인 후배에게도 감사의 말씀 드립니다. 일일이 언급하기 힘들 정도로 많은 도움을 주신 선후배님들 덕분에 지금의 제가 있을 수 있었던 것 같습니다. 제게 주셨던 모든 양보와 배려 그리고 인내에 보답 할 수 있도록 더욱 노력하겠습니다. 비록 저는 졸업하지만 ‘전지 및 전해공정 실험실’의 일원임을 절대 잊지 않겠습니다. 그리고 소중한 나의 인연, 원식이형, 우연인지 필연인지 대학원 생활까지 바로 옆에서 하면서 많은 도움 받았구만. 고마워. 그리고 또 다른 내 소중한 친구들 그리고 지인들, 모두 감사합니다. 변치 않는 모습 보여드릴게요.

그리고 무엇보다도, 어떤 것 보다도 소중한 저의 가족들. 2012년 5월 26일, 내 평생의 반쪽이 되어준 사랑하는 나의 부인 현주씨, 옆에서 항상 힘을 준 당신이 있어 내가 더 힘을 낼 수 있었던 것 같아. 고마워요. 대책없이 공부하겠다는 철없는 아들에게 아낌없는 무한한 지원을 해주신 부모님, 이기적으로 행동하는 철없는 동생에게 싫은 소리 한마디 않고 언제나 도와주던 누나 그리고 매형도 이 글을 빌어 감사하는 제 마음을 전하고 싶습니다. 모자란 사위를 항상 반겨주시고 사랑해 주시는 장인, 장모님께도 고개숙여 감사드립니다. 내가 바쁘다는 핑계로 결혼 후에 한번도 보지 못했지만 처제 그리고 동서도 고마워요. 그

리고 뱃속에 있는 우리 아기, 건강하게 자라서 우리 곧 만나자.

이제 저는 지금까지의 경험과 지식을 발판 삼아 새로운 도전을 시작하려고 합니다. 지금 이 글을 쓰는 동안 다시금 느꼈던 수많은 감사한 마음들과 각오들, 절대 잊지 않고 최선을 다해 나아가겠습니다. 지켜봐 주십시오. 여러분 모두들 감사합니다.

2012. 12.

화 윤 올림